

## Response to reviewers on the manuscript:

*Using ICESat-2 and Operation IceBridge altimetry for supraglacial lake depth retrievals* by Fair et al.

We thank the reviewers for their comments and suggestions to improve the clarity and structure of the manuscript. In this response, the original comment is given in black, the authors' response in blue, and the proposed changes in orange.

### **Response to Review #1**

Broad comment (1) “There are places outlined in the line-by-line comments where it could be more quantitative”

We addressed these suggestions on a case-by-case basis, as seen in the line-by-line responses below.

Broad comment (2) “Some of these sections are ‘in the weeds’ concerning HDF5 variable names or classification differences. These sections and figures could probably be excluded.”

We agree that Section 5.2 is too esoteric and technical in its current form. We assert, however, that this paper is a proof-of-concept study designed to highlight potential issues that a user may experience when performing automated supraglacial lake depth retrievals from ICESat-2 data. Therefore, while we propose to rewrite Section 5.2 to be less technical, we will retain a brief mention of the photon classification issues. The proposed rewrites are expanded upon in the responses to broad comments (3) and (4).

Broad comment (3) “I would expand on the section of difficulties of making a fully automatic lake depth detection algorithm with laser altimetry.”

As noted above, we plan to rewrite Section 5.2 to focus on the difficulties of automated retrievals from ICESat-2 data (Fricker et al., in prep.), with examples from the data formatting (i.e. photon classification) and from lake properties (bed topography, size, etc.), as follows:

#### **Section 5.2 Automation Challenges**

The identification of lake beds in the LSBS algorithm is based on a window of acceptable photons. The photon window is constrained by the coefficients  $a$  and  $b$  (for ICESat-2,  $a = 1.0$ ,  $b = 0.5$ ). Lake beds detected in this manner had a height uncertainty of 0.38 m (Table 2). The coefficients for ATM ( $a = 1.8$ ,  $b = 0.75$ ), resulted in more accurate retrievals on an individual basis. However, implementing varying  $a$  and  $b$  values proved difficult to automate, as other values may produce more accurate depths.

The challenges in full automation are related to three key issues. First, the observed extent of lakes varied considerably, especially over Greenland. The diversity in lake sizes complicated attempts to derive a universal “flatness” check. Smaller lakes present fewer lake surface photons, so a smaller data window ( $\sim 10^4$  photons) is required to prevent false positives. However, larger lakes may not be fully represented in smaller windows. A larger data window ( $\sim 10^5$  photons) will fully capture the largest lakes, but smaller lakes may then be overlooked.

Second, multiple scattering at the lake bed increases the photon spread and thus also increases the uncertainty of depth retrievals. Most supraglacial lakes observed by ATM featured smooth beds, so photons experienced one or few scattering events before returning to the detector. The instrument digitizer automatically filters return signals with low photon counts, reducing the spread of bed photons, at the cost of deep lake bottom detection. In contrast, the lakes observed with ICESat-2 exhibited more heterogeneous beds, leading to increased scattering events by photons and delays in return pulses. In these cases, the given values for  $a$  and  $b$  may not produce the most accurate bed solution. Furthermore, if the return is significant for a given photon window, then it may lead to a false negative for a portion of the lake (Figure 4i). To reduce uncertainty in lake depth retrievals, future improvements in working with ICESat-2 data should focus on identifying and filtering multiple scattering.

Finally, the ATL03 signal-finding algorithm is considered conservative in that it accepts false positives (background photons classified as signal photons) to ensure that all signal photons are passed to higher-level products (Neumann et al., 2020). Thus, uncertainties in the ATL03 photon classification contribute to noise in the water column and the lake bed. The classification algorithm uses surface masks to allocate statistical confidence to ATL03 photons for multiple surface types (Neumann et al., 2019b), with overlap possible among the surfaces. Melt lakes are too short-lived to be considered “inland water” and are instead categorized as “land ice” (lake surface) and “land” (lake surface and bed). Because the “land” classification also includes the bed, it includes more potential signal photons than land ice, so we recommend to only use land photons when performing supraglacial lake depth retrievals. It must be noted, however, that a lake bed profile is fully resolved only with the inclusion of low-/medium- confidence and “buffer” photons. The buffer photons ensure that all photons identified as surface signal are provided to the appropriate upper-level data product algorithms. However, they can introduce more noise to the profile, so more sophisticated filtering techniques are needed to distinguish the signal photons against the solar background.

Broad comment (4) “I would mention the impact of detector saturation on highly flat specular surfaces creating a “false” bottom return. This could be noted in the Algorithm Performance section.”

We agree that it is important to note the potential effects of specular reflection on observed lake surfaces. We will note its impact on lake depth retrievals in Section 5.1 as a potential obstacle.

A potential issue for lake depth retrievals concerns specular reflection. When photons interact with a flat water surface, they may reflect directly back to the detector with minimal energy loss.

The excessive return energy produces a “dead time” in the ATLAS detector, and the return signal is represented by multiple subsurface returns approximately 2.3 m and 4.2 m below the true surface (Neumann et al., 2020). An example of this phenomenon may be seen in Fig. 4f, where a prominent subsurface return is featured along the lake extent. However, because the subsurface echo is smaller than the true surface when viewed through histograms, the LSBS algorithm is able to avoid biases caused by specular reflection.

Page 1, Lines 2-4: “I would split this sentence to be something like: ‘Detection of lake extent, depth, and temporal evolution is important for understanding glacier dynamics. Previous remote sensing observations of lake depth are limited due to inherent uncertainties of depth retrievals with passive remote sensing techniques, and the high absorption of infrared laser energy in water from the original ICESat mission.’”

We changed as requested with a slight edit, as we do not see it necessary to mention ICESat here:

...for understanding glacier dynamics. Previous remote sensing observations of lake depth are limited to estimates from passive satellite imagery, which has inherent uncertainties, and there is little ground truth available.

Page 1, Line 8: “I would change this to reliably or statistically detect lake beds as deep as 7m.”

We made the following change:

Both lidars reliably detect lake beds as deep as 7 m.

Page 1, Line 10: “The insufficient classification of photon events when profiling lakes is expected due to how the ATL03 classification algorithms work with a bimodal or multimodal surface, particularly if the lake surface return is not specular.”

The statement given here is addressed to a general scientific audience that may not be aware of the ATL03 classification algorithms. However, we agree it is to be expected, so we will reword the text as follows:

The bimodal nature of lake returns means that high-confidence photons are often insufficient to fully profile lakes, so lower confidence and buffer photons are required to view the lake bed.

Page 1, Line 16: “You are noting here that the contributions to sea level rise from ice sheets will likely overtake steric sea level effects and not that the contributions will overtake glacier and ice caps correct?”

You are right. To make this clearer, we reworded the statement as:

...leading to the contributions from both ice sheets to overtake the contribution of thermal expansion to sea level rise (Vaughan et al., 2013).

Page 1, Line 17: “I would probably use ‘aggregation’ and not ‘accumulation’”.

We changed as requested:

Meltwater plays vital roles in ice sheet evolution [...], including aggregation on ice sheets as supraglacial lakes.

Page 1, Line 18: “When unfrozen, these lakes exhibit a lower albedo than the surrounding ice,”

We changed as requested:

When unfrozen, these lakes exhibit a lower albedo than that of the surrounding ice...

Page 1, Line 21: “which can lead to potentially significant impacts”

We changed as requested:

...their spectral emissivity in the IR spectrum also differs from bare ice [...], which can lead to potentially significant impacts...

Page 2, Lines 2–4: “Meltwater penetration into the ice during catastrophic lake drainage events can also lead to hydrofracture, a mechanism through which meltwater facilitates full ice fracture as a result of the stresses induced by the density contrast between liquid water and ice”

We applied the following change:

During catastrophic lake drainage events, meltwater penetration into the ice can also lead to hydrofracture...

Page 2, Line 5: “thus can impact sliding velocity and ice discharge”

We changed as requested:

...which in turn modify the resistance to ice flow and thus can impact sliding velocity and ice discharge.

Page 2, Line 12–13: “Hopefully we don’t reach a time where supraglacial lakes are present over the entirety of either ice sheet. ‘sheer size of the ice sheet ablation areas’”

We agree. We applied the following change:

However, the harsh conditions of Antarctica and Greenland, the transience of meltwater, and the sheer size of the ice sheet ablation zones...

Page 3, Line 4: “6 distinct beams named in the products based on the ground track: GT1L/R, GT2L/R, and GT3L/R.”

We applied the following change:

...a 532 nm micro-pulse laser that is split into six distinct beams with names based on the ground track...

Page 3, Line 6: “approximately every 0.7 meters”

We changed as requested:

...ICESat-2 records a unique laser pulse approximately every 0.7 m...

Page 3, Line 16: “GT2R can be either the central strong beam or the central weak beam based on the orientation of the spacecraft. For the both of your dates (2019-01-02 and 2019-06-17) GT2R was the weak beam.”

You are correct. We edited the text to fix this mistake:

Of the six beams available, we concentrated on the central strong beam (GT2L)...

Page 3, Lines 18–20: “This is expected due to transmit pulse truncation. The transmit pulse shape is slightly non-Gaussian with a trailing tail. Calculating the average of photon events without that trailing tail biases the results compared to a ‘true’ surface.”

We respond to the reviewer assuming that they are referring to the inclusion of lower confidence photons. With this assumption, we added the following:

The addition of medium, low, and “buffer” photons slightly decreases measurement precision, but a less truncated transmit pulse gives better agreement with ATL06 and ground-based data (Brunt et al., 2019b).

Page 3, Lines 21–22: “Versions of ATM have flown in Greenland since 1993. As written it suggests that ATM was designed as a gap filling instrument rather than an existing and verified instrument suite used in this role.”

We agree. To make it clearer that we are referring to the IceBridge measurements, we applied the following changes:

The Operation IceBridge (OIB) campaign was designed to fill the gap in polar altimetry between ICESat and ICESat-2. Its scientific payload included the Airborne Topographic Mapper, a 532 nm lidar that has been used for ice sheet and shallow water measurements since 1993.

Page 3, Line 25: “The ATM1B QFIT elevation product is not a geolocated photon product but a geolocated elevation product”

You are correct. We applied the following change:

The ATM Level-1B Elevation and Return Strength (ILATM1B) product converts analog waveforms into a geolocated elevation product...

Page 3, Line 26: “While ATM does not contain a statistical confidence definition, ATM uses a thresholded centroid model from their digitized waveforms and thus will typically only retrieve higher confidence returns. The data is also processed prior to release for QA/QC purposes.”

The thresholding applied to ATM data is briefly mentioned in Section 4, but it is in the context of poor signal return for deep lake beds. To highlight the benefits of the centroid model, we added information to Section 5.2 (see response to broad comment #3), and reworded Line 26 as:

...to emulate ATLAS data (Studinger, 2013, updated 2018). Although it lacks a statistical confidence definition, ATM applies a centroid model to digitized waveforms and to retrieve high-confidence photons.

Page 3, Line 26: “Remove ‘Despite this’”

We changed as requested:

...retrieves high-confidence photons. Brunt et al. (2019a) found that...

Page 3, Lines 27–28: “Here, the ATM results serve as a proof of concept for the lake detection algorithm”

We changed as requested:

Here, the ATM results serve as a proof-of-concept for the lake detection algorithm.

Page 4, Lines 4–5: “The lake surfaces aren’t necessarily “easily” identifiable and potential lake beds can be hard to detect on highly flat surfaces because detector saturation (related to first-photon-bias) can lead to a non-existent false bottom.”

We acknowledge that lake surfaces can be difficult to discern from other features (i.e. smooth ice in close proximity to the lake, so we removed the assertion that surfaces are “easily” identifiable. We elaborate on the effects of specular reflection in the revised Section 5 (see above).

...with the expectations that (i) lake surfaces would be identifiable in photon histograms and (ii) lakes may be found via statistical inference in the region of the lake surface.

Page 4, Lines 5–6: “To simplify the identification of lake features, we separated them into two arrays: one for the surface and one for the bed, which we refer to as ‘lake surface-bed separation (LSBS).’”

We changed as requested:

...one for the surface and one for the bed, which we refer to as “lake surface-bed separation” (LSBS).

Page 4, Line 8: “What is  $\sim 10^4$ – $10^5$  photons in terms of distance?”

The given number of photons is equivalent to  $\sim 1$ - $10$  km in along-track distance for ICESat-2 and  $\sim 0.15$ - $1.5$  km for ATM. We added the following to provide context:

We divided each data granule into discrete along-track windows to reduce the data volume to  $\sim 10^4$ - $10^5$  photons per window. This photon count is equivalent to  $\sim 1$ - $10$  km in along-track distance for ICESat-2 and  $\sim 0.15$ - $1.5$  km for ATM.

Page 4, Line 11: “Are there times when the lake bottom can be the dominant return?”

Yes - this issue may be observed in Figure 4i, where a strong bottom return in a shallow lake leads to a false negative over part of the lake. We added commentary on this observation in Section 5.

The given values for  $a$  and  $b$  may not produce the most accurate lake bed solution in these cases. Furthermore, if the bottom return is significant for a given photon window, then it may lead to a false negative for that portion of the lake (Figure 4i).

Page 4, Line 12: “We check the flatness of the window by computing the standard deviation”

We propose this change, as requested:

We check the flatness of the window by computing the standard deviation of high-confidence signal photons...

Page 4, Lines 23–24: “Seems somewhat arbitrary that the thresholding needed to be different surface classification. Would it be better to only use the full set of potential signal photons and the second set of thresholds?”

We agree that ICESat-2 photons do not require thresholds based on classification. Most lakes we considered required medium-/low- confidence and buffer photons, so we applied the second threshold to all cases. The statistics given in Table 3 reflect this thresholding.

However, the second threshold proves ineffective for shallow lakes in ATM data, whereas the first threshold was applicable in all cases. Therefore, to improve readability, we propose to remove the procedural step starting at Line 23, and revised Lines 19-22 to be:

Within these horizontal bounds, photons were defined as a lake bottom if they satisfied the condition:  $h_{sfc} - a\sigma_{sfc} \leq h \leq h_{sfc} - b\sigma_{sfc}$ , where  $\sigma_{sfc}$  is the standard deviation of lake surface photons. The constraints  $a$  and  $b$  were derived through trial-and-error, such that  $a = 1.0$  (1.8) and  $b = 0.5$  (0.75) for ICESat-2 (ATM). We set these constraints to reduce the impacts of multiple scattering and specular reflection on depth estimates.

Page 4, Line 30: “I would say that these were ‘potential’ or ‘probable’ false positives.”

We propose to apply the following change:

If the number of bed photons was very small (100 or less), then the scene was marked as a probable false positive.

Page 5, Line 6: “overlapping 40 meter segments”

We changed as requested:

...ATL03 photon aggregates within overlapping 40 m segments...

Page 5, Paragraph 2: “The ATL06 algorithm assumes a single returning surface within a segment of photon events. In supraglacial lake instances, the ATL06 algorithm can compute a height for either lake bottom or lake surface depending on their corresponding return strength. These return strengths can be highly variable.”

We thank the reviewer for providing their knowledge of the ATL06 algorithm. In response, we revised Paragraphs 2 and 3 in the following manner:

The linear regression in ATL06 accounts for all ATL03 photons (background or signal), and the technique performs a background-corrected spread estimate to narrow the range for acceptable photons. This is an iterative scheme; the refinement process repeats its acceptable photon filter

until no photons are removed. As a consequence, the ATL06 algorithm assumes a single returning surface, so over a melt lake it will compute a height for either the lake bottom or the lake surface, depending on their return strengths.

The condition for acceptable surface photons in ATL06 is given by:

$$|r - r_{med}| < 0.5H_w$$

Within a 40 m photon segment,  $r$  is the residual of a photon relative to the linear regression,  $r_{med}$  is the median residual, and  $H_w$  is window height. The height of the window is taken as the maximum of the observed photon spread, the window height (if any) and 3 m, and photons within the window range are defined as the surface. The LSBS algorithm follows a similar procedure, but the flatness of the lake surface and relatively low photon density of the corresponding beds rendered iterating unnecessary. The lake bed is then defined as photons not within the window and below the surface...

Page 5, Line 18: “The ATL06 algorithm uses 3m as the minimum window height.”

You are correct. We applied the following correction:

The height of the window is taken as the maximum of the observed photon spread, the previous window height (if any), and 3 m...

Page 5, Line 26: “I would mention that 3cm is far below the horizontal geolocation uncertainty of ICESat-2”

To highlight the accuracy of ICESat-2 geolocation, we applied the following change:

The central strong beam for ICESat-2 is near-nadir, so the horizontal offset was determined to be small relative to the size of lakes (~3 cm, far below the horizontal geolocation uncertainty of ICESat-2).

Page 6, Line 10: “What do you mean quantitatively by agree well?”

We acknowledge that a quantitative representation of the agreement would be beneficial. We therefore made the following change:

We compare  $z_s$  and  $z_p$  over lakes with well-defined bottoms, and show in Sect. 4 that the two generally agree to within 0.88 m.

Page 6, Lines 12–14: “These sentences are awkwardly phrased.”

We reworded the given sentences in the following manner:

We acknowledge the desire to retrieve lake volume from laser altimetry, but we leave the development of such an algorithm for a future study. For example, depth retrievals from ICESat-2 could potentially be combined with lake radius and shape estimations determined from visible satellite imagery to derive water volume.

Page 6, Lines 16–18: “You list the dates here, in Figure 1 and in Table 1. I would get rid of Table 1 as it seems extraneous.”

We assessed the necessity of Table 1, and we agree that it is redundant with the information given in Section 3.4. The table is deleted in the revised manuscript. Lines 19-20 were changed to reflect this:

Comparisons between Landsat-8 imagery and ICESat-2/OIB flight tracks confirmed supraglacial lake overpasses for study. In Spring 2019...

Page 6, Lines 21–23: “Why mention this?”

At the time of writing, ATM data from the 2019 Spring campaign were unobtainable despite the availability of ICESat-2 data. Lines 21-23 are given as justification for the lack of case studies co-located by ICESat-2 and ATM. With the release of the 2019 Spring data, we were unable to find suitable lake candidates that may be observed by both ATM and ICESat-2. We updated the given lines to reflect this:

There were no lakes sampled at the time by both ICESat-2 and OIB.

Page 6, Lines 25–26: “I would rewrite to be ‘We detected 12 lakes with sufficient bed returns from the ATM data and 16 potential lake surfaces overall.’”

We changed as requested:

We detected 12 melt lakes with sufficient bed returns from the ATM data and 16 potential melt lake surfaces overall. The melt lake profiles are shown in Fig. 3...

Page 6, Line 27: “What do you mean quantitatively by good accuracy?”

We qualitatively considered the surface accuracy to be “good” if the algorithm distinguished between lake surfaces and the surrounding ice terrain. To provide a more quantitative assessment, we calculated the standard deviation of surface photons ( $\sigma_{sfc}$ ). The mean for  $\sigma_{sfc}$  was found to be 0.0087 m, thus demonstrating the effectiveness of the flatness check. We revised Line 27 to reflect this assessment:

The algorithm reliably distinguishes between lake surfaces and the surrounding ice terrain. The mean spread among lake surface photons is 0.0087 m, or well within the flatness threshold of 0.02 m. Lake bottoms are well-defined when  $d_s < 8$  m. Lake bottoms deeper than 8 m exhibit fewer signal returns...

Page 7, Line 3: “lake bed elevations”

We changed as requested:

The highest uncertainties are observed for lake depths greater than 3 m...

Page 7, Line 4: “perhaps influenced by low signal-to-noise ratios or the conical scanning of the lidar instrument”

We changed as requested:

...perhaps influenced by low signal-to-noise ratios or the conical scanning of the OIB lidar instrument.

Page 7, Lines 8–9: “We examined an additional 12 supraglacial lakes with ICESat-2, eight in Greenland and four highlighted in Magruder et al. (2019) on the Amery Ice Shelf in Antarctica (Fricker et al., in prep.)”

We applied the following change:

We examined an additional 12 supraglacial lakes with ICESat-2, eight in Greenland and four highlighted in Marguder et al. (2019) and Fricker et al. (in prep) on the Amery Ice Shelf in Antarctica.

Page 7, Line 10: “What do you mean by reasonable success?”

As with Page 6, Line 27, “reasonable success” is a qualitative assessment of the lake surface/bed profiles. We added a quantitative assessment of lake surface/bed uncertainty, as seen below.

The refined algorithm captures lake surfaces and beds reasonably well (Fig. 4), with a mean uncertainty of 0.015 m for surface photons and 0.38 m for bed photons.

Page 7, Line 21: “less necessary for ICESat-2 than ATM for the supraglacial lakes studied here”

We changed as requested:

It must also be noted that lake bed photons are more likely to be found in the ATL03 photon cloud than in ATM waveforms, meaning that the polynomial estimates are less necessary for ICESat-2 than ATM for the supraglacial lakes studied here.”

Page 7, Line 34: “ICESat-2 returns are also affected by first-photon-bias (particular if complete saturation of the detectors occurs), blowing snow events (which by forward scattering can create sub surface photons or have a multi-modal return by the snow itself), and solar radiation background.”

The reviewer is correct. To highlight these issues, we revised Line 33 to include the following:

At its operational altitude, the ATLAS laser is subject to first-photon-bias, solar background radiation, and scattering and absorption by clouds and blowing snow.

Page 8, Line 7: “What do you mean in the attribution sentence?”

In lakes observed by ICESat-2, we observed clear differences in lake bed topography between Antarctica and Greenland. We speculate in the revised Section 5.2 that bed topography may affect the return signal of the ATLAS laser and produce greater uncertainties.

We also realized that the sentence did not flow with the preceding paragraph, so we propose to revise the sentence as follows:

We observed differences in lake topography for ICESat-2 lakes, and we attribute them to the underlying ice surfaces.

Page 8, Lines 14–31: “I’m not sure if mixing classifications is the best approach for determining the signal classification. You’re right that supraglacial lakes are not quite fit in any default category in the signal classification algorithm of ATL03. I may be mistaken but I think supraglacial lakes being classified higher in “land” than “land ice” makes sense due to the tighter histogram window of “land ice” (and not that supraglacial lakes resemble canopies). Going forward, it might be better to use signal and buffer photons of a single surface class and iterate to remove potential background photons.”

We agree that a single surface class offers a simpler approach to the classification issue discussed in Section 5.2. A follow-up analysis confirmed that the “land” classification is sufficient to characterize the lakes examined in this study. The example given in Figure 5 highlights this point.

According to the ATL03 Algorithm Theoretical Basis Document, classifications are based on surface masks, with overlaps frequent for land and land ice over ice sheets. Therefore, differences between the two surface types should originate from dissimilar criteria for signal

photons, as the reviewer suggests. To amend this misconception, we edited the following for the revised Section 5.2 (see broad comment #3):

Finally, the ATLO3 signal-finding algorithm is conservative in that it accepts false positives (background photons classified as signal photons) to ensure that all signal photons are passed to higher-level products. Thus, uncertainties in the ATLO3 photon classification contribute to noise in the water column and the lake bed. The classification algorithm uses pre-defined surface masks to allocate statistical confidence to ATLO3 photons for multiple surface types (e.g. “*inland water*”, “*land ice*”, “*land*”; Neumann et al., 2019b), with overlap possible between masks. Melt lakes are categorized as “*land ice*” (lake surface) and “*land*” (lake surface and bed). Because the “*land*” classification also includes the bed, it includes more potential signal photons than *land ice*, so our recommendation is to only use *land* photons for supraglacial lake depth retrievals. It must be noted, however, that a lake bed profile is fully resolved only with the inclusion of low-/medium- confidence and “buffer” photons. The buffer photons ensure that all photons identified as surface signal are provided to the appropriate upper-level data product algorithms. However, they can introduce greater noise to the profile, so more sophisticated filtering techniques are needed to distinguish between signal photons and the solar background.

Page 9, Line 7: “Should add a value for ‘too deep’”

We agree. For better consistency with the results, we changed Line 7 to the following:

Lake bottoms are easy to identify once lake surfaces are established, given that the lakes are not deeper than 7 m.

Figure 4: “The polynomial fits are pretty poor for complex beds. I get the need to not overfit the beds, but would it be better to use a variable order of polynomial or splines?”

It is true that the polynomials perform poorly for many of the lakes observed by ICESat-2. The 3<sup>rd</sup>-order approximation was designed to fill the gaps in deep lakes with the classic “bowl” shape. The polynomial fits therefore perform most effectively for the deep lakes observed by ATM, where the bed topography is less complex.

The lake beds in Figure 4 generally show greater complexity, which results in the poorer fits. In these cases, we agree that a spline interpolation would perform more effectively. We therefore replaced the polynomial fits in Figure 4 with splines on a case-by-case basis. Ultimately, only the polynomial fit in lake 4i was retained due to poor spline fitting.

We highlight the notion that the polynomial/spline fit is less unnecessary for ICESat-2 lakes, given that bed photons are more likely to be found in the ATLO3 photon cloud. Its primary function in ICESat-2 retrievals is to fill gaps missed by the initial bed-finding routine, rather than predict the deepest part of lakes. Due to the limited usage of the 3<sup>rd</sup>-order fit, we removed the “polynomial error” column in Table 3, instead focusing on how the interpolants improved retrievals for lakes 4a, 4b, 4f, and 4i. The updated Figure 4 is shown below.

Lastly, the change to spline fitting for ICESat-2 lakes necessitated alterations to the text. The changes are given here:

Page 6, Paragraph 2: For deep or inhomogeneous lakes, attenuation of photon energy in water resulted in fewer signal photons observed at lake bottoms (Fig. 4). In these situations, we fitted polynomial or spline fits to all lake profiles with bounds at the lake edges. Lakes observed by ATM typically featured “bowl” shapes and attenuation at the deepest parts, so 3<sup>rd</sup>-order polynomials were sufficient. In ICESat-2 data, the retrieved lake beds showed greater complexity, so we tested polynomial fits and splines on a case-by-case basis. Lake depths approximated with curve fitting were denoted as  $z_p$ ...

Page 7, Lines 17-21: The curve fits improved depth estimates for lakes 4b, 4f, and 4i. Of these lakes, only 4i used a polynomial estimate due to poor spline fitting. The inclusion of interpolants increased the mean depth estimates of 4b, 4f, and 4i by 0.08 m, 0.04 m, and 0.03 m respectively. The spline fitting also significantly increased the maximum observed depth in lake 4b from 2.67 m to 3.27 m. The remaining lakes featured more complete bed profiles, meaning that the fitting estimates were less necessary.

Figure 4: Polynomial curves were replaced with splines. The legend entry “Polyfit” was changed to “CurveFit” (this change also occurred for Figure 3).

Table 3: The polynomial error ( $\epsilon_p$ ) was removed.

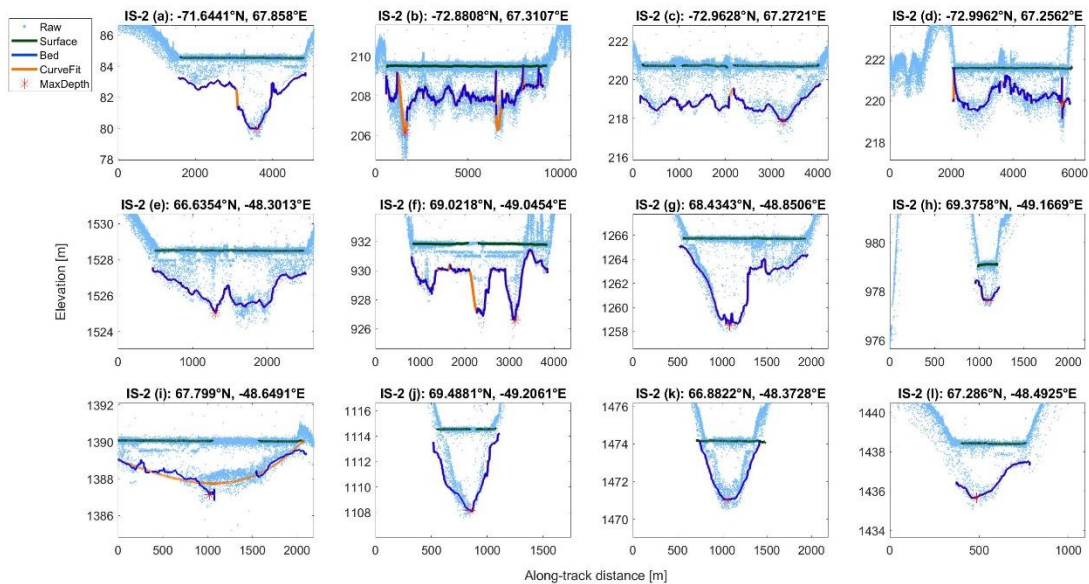


Figure 4. Supraglacial lakes and melt ponds detected by ICESat-2 over the Amery Ice Shelf (a-d, reported by Magruder et al., 2019 and Fricker et al., in prep.) and western Greenland (e-l), using Tracks 0081 and 1222, respectively.

Figure 4: “Bed detection seems to be a bit off on the lake edges (a, e, g, i, j, k, l).”

The lake bed detection is restricted to the edges of the lake surfaces. This limitation affects the number of photons considered to be acceptable bed photons, which occasionally leads to a slight skewing of the lake bed near the edges. We observed this issue occurring most frequently with smaller, shallower lakes with fewer photons. The following was added to Lines 9-11 to account for this:

The refined algorithm captures lake surfaces and beds reasonably well (Fig. 4), with a mean uncertainty of 0.015 m for surface photons and 0.38 m for bed photons. The lake edges partially account for the bed photon uncertainty, for the limited number of acceptable photons produces a slight bias in bed estimates.

Figure 5: “I don’t know if this figure has much meaning.”

After careful consideration, we agreed that Figure 5 is unnecessary for the relevant discussion. We propose to delete it.

Table 1: “I don’t think this table is necessary with Figure 1 and the text.”

As mentioned in a previous comment, we removed Table 1 and made the appropriate text changes.

## **Response to Review #2**

Scope comment: “The paper limits itself to central strong beam (GT2R), but then also includes lower confidence photos from this band which ‘decreases measurement precision but gives better agreement with ground-based data.’ Because of this, I am wondering why other beams were not used, or at least their potential use discussed in the paper?”

The central strong beam was initially selected for the number of lakes observed over the Amery Ice Shelf. However, we recognize that the other strong beams (GT1L and GT3L) could also be used for depth retrievals. The weak beams (GT1R, GT2R, and GT3R for these ground tracks) are less effective at detecting beds for deeper lakes, so they were omitted from this study. We added the following to Section 2.1 to address these questions:

Our study focused on the central strong beam, as the number of lakes was deemed sufficient for our purposes. While we recognize that the other strong beams could be useful for depth retrievals we did not consider them here. We speculate that the weak beams may avoid issues with multiple scattering and specular reflection, but their power is too low to reliably detect lakes deeper than 4 m.

Page 6 Line 14: “Do you have any estimate for just how widely applicable these methods will be / how easy it is to get good coverage? I understand you have to put limits on this paper

somewhere, for sure, so this is mostly out of curiosity and might be of interest in a discussion/conclusion?”

We agree that these points would be useful to readers, so we added more information in Section 5.1.

The success of this method for lake depth retrievals is governed by spatial and temporal sampling of the instruments across the lakes when they are full. The methods presented here are most effective when the altimeter passes directly over the deep part of a lake rather than at its edge. This provides a lake depth profile that is more representative of the complete lake, allowing for improved estimates of lake depth and extent. A complete lake profile also provides sufficient information to the LSBS algorithm, reducing the risk of false negatives that occur with small lakes or incomplete profiles. The temporal sampling of ICESat-2 and ATM is infrequent (every 91-days for ICESat-2 and random for ATM), and so the same lakes will not always be present every time these data are required. Therefore, coincident satellite imagery is desirable to simplify the lake-finding process.

Data & Code Citation/Sharing (1) “The Cryosphere’s data policy states that ‘Authors are required to provide a statement on how their underlying research data can be accessed. This must be placed as the section ‘Data availability’ at the end of the manuscript.’ I did not see such a section. Clarity in citing the exact subsets of the large datasets that you cite would be ideal (which I know is also in your Table 1, but not presented in one place).”

The full information for the ICESat-2 and ATM data is given in Section 3.4, including date, ground track number, and coordinates. However, we acknowledge the lack of a Data Availability section, and we included one in the revised manuscript.

Code and data availability: ICESat-2 ATL03 V002 and ATM L1B V002 data may be accessed from <https://doi.org/10.5067/ATLAS/ATL03.002> and <https://doi.org/10.5067/19SIM5TXKPGT>, respectively. Depth data for the supraglacial lakes given in Figure 4 are available at <https://doi.org/10.5281/zenodo.3838274>. Depth data for lakes in Figure 3 are available upon request from Zachary Fair. The LSBS algorithm and its subroutines may also be accessed from <https://doi.org/10.5281/zenodo.3838274>.

Data & Code Citation/Sharing (2) “The Cryosphere guidelines also state that “Data do not comprise the only information which is important in the context of reproducibility. Therefore, Copernicus Publications encourages authors to also deposit software, algorithms, model code, video supplements, video abstracts, International Geo Sample Numbers, and other underlying material on suitable FAIR-aligned repositories/archives whenever possible. These materials should be referenced in the article and cited via a persistent identifier such as a DOI.” There is clearly a lot of important code developed and used by the authors, and it would be in line with this journal’s goals that it be documented, shared, and cited. This would allow for reproducibility, further application of these methods, and further refinement, as well. I very

much hope that the reviewers document, share, and cite the final version of their code to make their methods as open as the data they use and the publication they have chosen to publish in. (Of course, if you have another code/methods paper in prep, then please do cite that and I apologize for jumping the gun!)”

The lake detection algorithms are available under the Assets section through the following link: <https://doi.org/10.5281/zenodo.3838274>. This is noted in the “Code and data availability” section.

The LSBS algorithm and its subroutines may also be accessed from the DOI given above.

Data & Code Citation/Sharing (3) “And since I’m talking about data and code sharing - at the risk of inviting my own citation - you cited Pope et al 2016 on Page 2 Line 23/24. I wonder whether you might (also) want to cite Pope (2016), which I bring up here because it more fully describes, documents, and shares the code developed and used in the Pope et al paper. <https://doi.org/10.1002/2015EA000125>”

We agree that the given paper would be a useful citation. We therefore added the following to Page 2, Line 17:

The normalized water difference index (NWDI) and dynamics thresholding techniques have also been considered for lake detection (Fitzpatrick et al., 2014; Liang et al., 2012; Moussavi et al., 2016; Pope, 2016; Williamson et al., 2017; Moussavi et al., 2020).

Page 1 Line 8-9 (Abstract): “Can you quickly mention where the uncertainties are derived from here? It might just be me, but if quickly reading, it makes it sound like there is comparison to some in situ data...”

The uncertainty was derived from the standard deviation of acceptable lake bed photons. In other terms, the depth uncertainty is equal to the spread of lake bed photons. We reworded the given lines to be clearer:

Lake bed uncertainties for these retrievals...

Page 4 Line 10: “about how long is each data granule, in ground distance, to include  $10^4$  -  $10^5$  photos per window? I think this will help people understand the next assumptions.”

Each flight track for ATM is 13-15 km in length, whereas each ICESat-2 ground track is  $\sim 10^3$  km in total distance. We indirectly addressed this comment in response to Reviewer #1:

We divided each data granule into discrete along-track windows to reduce the data volume to  $\sim 10^4$ - $10^5$  photons per window. This photon count is equivalent to  $\sim 1$ - $10$  km in along-track distance for ICESat-2 and  $\sim 0.15$ - $1.5$  km for ATM.

Page 4 line 14: “How were these ranges selected / chosen? This would seem to be an important part of method development.”

These thresholds were selected by comparing the flatness of lake surfaces to that of surrounding ice topography. We also note here that the ATM threshold of 0.002 m was a typo, and it is supposed to be 0.02 m. We added the following to provide more clarity:

We define a “flat” surface for regions where  $\sigma \leq 0.05$  m for ATL03 data, and  $\leq 0.02$  m for ILATM1B data. We selected these values by comparing the “flatness” of lake surfaces to that of surrounding ice topography.

Page 4 Line 14: “I’m sorry if I missed it, but can you define sigma in the text upon first usage?”

Sigma is previously defined as the standard deviation of high-confidence photons in Lines 12-13. To avoid confusion for future readers, we edited these lines slightly:

We check the flatness of the window by computing the standard deviation ( $\sigma$ ) of high-confidence signal photons...

Page 4 Line 17: “Consider replacing "lake surface" with ‘height of the lake surface’ and underlining the letters h, s, f, and, c in order to make the abbreviation very clear?”

We changed as requested:

...we assigned the data to a new array for the height of the lake surface ( $h_{sfc}$ ).

Page 4 Line 20: “How were these ranges selected / chosen? This would seem to be an important part of method development.”

The ranges for acceptable bed photons were selected through trial-and-error. The given bounds were selected to minimize the impacts of multiple scattering and specular reflection. To make this clear in the text, and to address comments from Reviewer #1, we reworded Lines 19-22 to be:

Within these horizontal bounds, we defined photons as a lake bottom if they satisfied the condition:  $h_{sfc} - a\sigma_{sfc} \leq h \leq h_{sfc} - b\sigma_{sfc}$ , where  $\sigma_{sfc}$  is the standard deviation of lake surface photons. The constraints  $a$  and  $b$  were derived through trial-and-error, such that  $a = 1.0$  (1.8) and

$b = 0.5$  (0.75) for ICESat-2 (ATM). We set these constraints to reduce the impacts of multiple scattering and specular reflection on depth estimates.

Page 4 Line 22: “Consider replacing ‘lake surface’ with ‘height of the lake bottom’ and underlining the letters h, b, t, and, m in order to make the abbreviation very clear?”

We assume this is a typo and that the reviewer is actually requesting a rewording of the term “lake bottom” (rather than “lake surface”). With this assumption, we applied the following change:

...the data were placed in an array for the height of the lake bottom ( $h_{btm}$ ).

Page 4 Line 27: “How were these filters chosen? This would seem to be an important part of method development.”

We expand upon these issues in Section 5.2. However, we acknowledge that justification is needed here, so we applied the following change:

For ICESat-2, lakes shallower than 1.3 m or less than 200 m in horizontal extent were found to be too noisy or ill-defined for further analysis (see Section 5.2 for more details).

Page 4 / Section 3.1 in general: “It would be even clearer to present these methods if there were agreement between the steps here and in Figure 2 (e.g. one box / arrow per bullet point).”

We contemplated this suggestion, and we decided that one box or arrow per bullet point was unnecessary. However, we added labels to Figure 2 (now Figure 1 in response to another suggestion) to improve consistency with Section 3. The modified figure is shown below, and the bullet points in Section 3.1 were changed for consistency:

- i. We divided each data granule into discrete along-track windows...
- ii. Each data window was binned into elevation-based histograms...
- iii. If the satellite image(s) confirmed the presence of a lake, the data were assigned to a new array for the lake surface ( $h_{sfc}$ ). The horizontal extent of the lake surface served as a constraint for where the lake bottom data could be defined...
- iv. A series of filters were applied to improve surface/bed estimates...
- v. If the data were obtained from ICESat-2, then we followed a photon refinement routine that is described in more detail in Section 3.2. Calculations for lake depth were then performed for both ATM and ICESat-2 retrievals and corrected for refraction (Section 3.3).

Page 6 Line 18: “I could be wrong, but it is possible that Figure 1 and 2 are cited in backwards order? You might consider flipping their numbers?”

You are correct. For better consistency, we changed the numbering for the relevant figures.

(From Page 4, Line 7) For both instruments, the procedure for separation was identical, and is as follows (see Fig. 1 for a schematic view)...

(From Page 6, Lines 16-18) We present cases over the Amery Ice Shelf [...], the western Greenland ablation zone [...], and Hiawatha Glacier [...] (Fig. 2).

Page 5 Line 27: “You mention a refraction correction but then there is no further detail. I know it is pretty basic, but for full clarity perhaps describe slightly more / provide a citation for the method you use for refraction correction?”

The refraction correction mentioned in Line 27 is briefly described in Lines 23-25. Line 24 includes a citation to Parrish et al. (2019), who outline a refraction correction algorithm based on beam angle and water depth. For quick reference, the passage is given below:

As a final adjustment to the lake photons, we applied a refraction correction algorithm to account for slowing down of the light as it enters water. The correction follows the methods utilized by Parrish et al. (2019) by approximating refractive biases as a function of depth and beam elevation angle.

Page 6 Line 29: “I wonder if you this it is important to re-emphasize the filtering of which lake depths were kept in presenting average lake depths? e.g. lots of shallow lakes aren’t being included?”

The lake statistics given in Table 2 reflect quantities calculated from the lakes included in Figure 3. Therefore, the excluded lakes were not considered for the average depth given in Line 29. To emphasize this, we reworded Line 29 to be:

The average lake depth estimate for the lakes in Fig. 3 was 1.95 m...

Figure 1: “Consider using dots to indicate location, rather than ovals, which are much larger than the image are?”

This is a good suggestion. We replaced ovals with stars centered on the regions of interest. The stars appeared small if the full continental image was used, so we cropped the images to center on the markers. The new figure may be seen below:

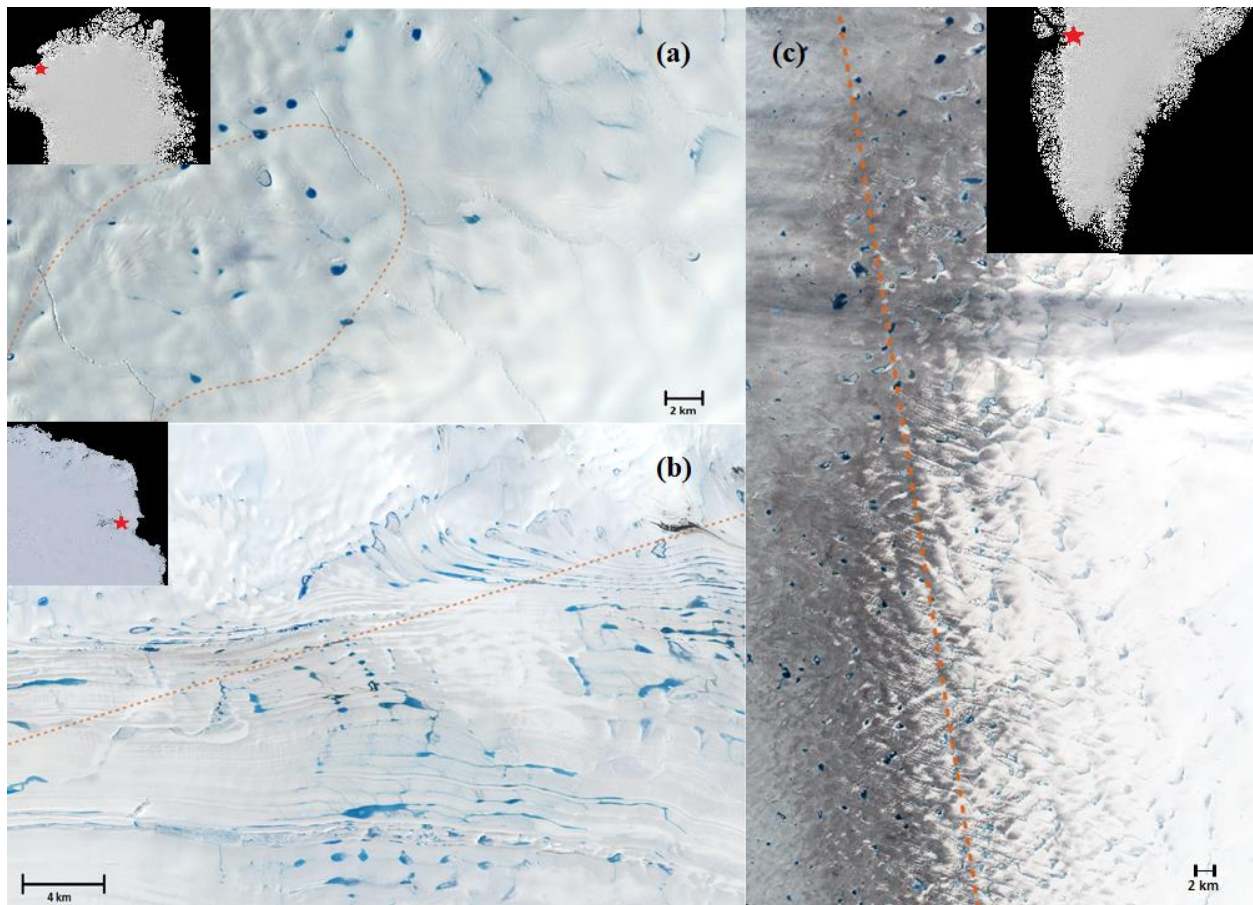


Figure 2: “It is slightly confusing that you use the same blue boxes for both data and processes (e.g. Landsat 8 imagery vs verify lake detection), consider using different shapes / colors / some design choice to indicate the difference?”

We changed the color of the “ATL03/ILATM1B granule” and “Landsat-8 imagery” boxes to green to differentiate data inputs from algorithm steps. We also grouped the steps into sections to create better consistency between the figure and Section 3, as suggested above. The new figure and caption are shown below:

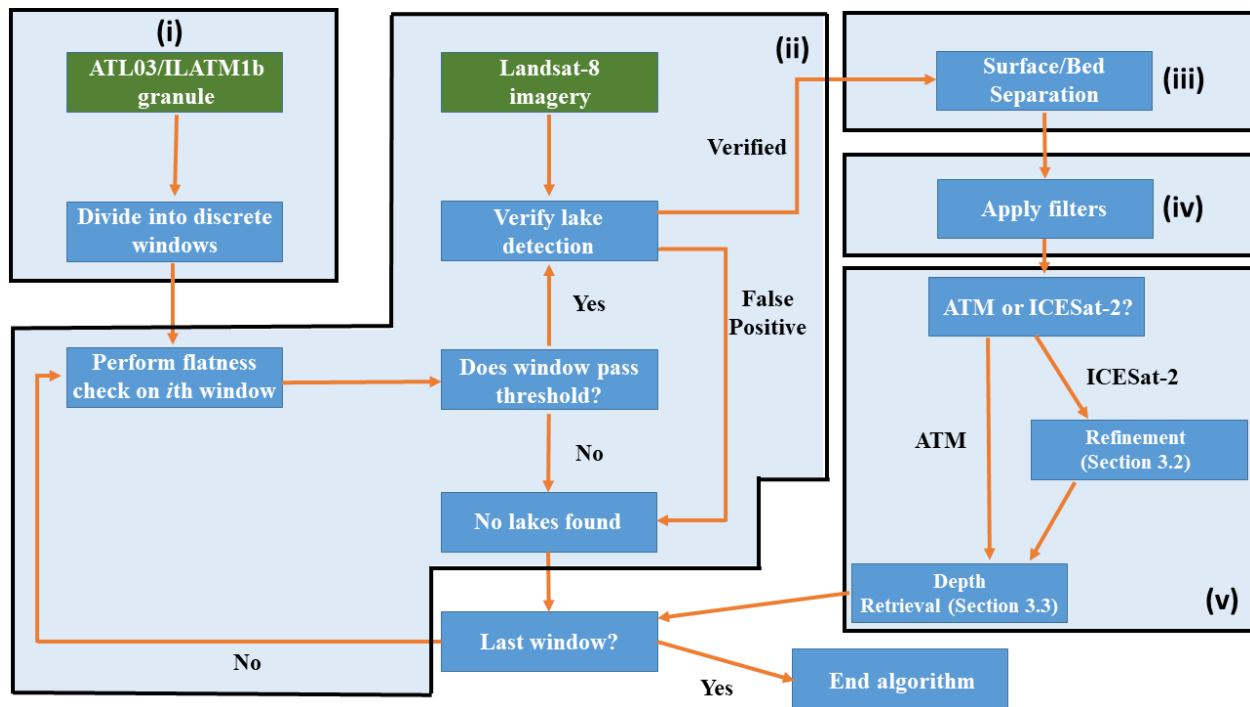


Figure 2. Schematic for the workflow of the lake surface-bed separation algorithm, where green boxes indicate data inputs and blue boxes are steps in the algorithm. Roman numerals match the steps given in Section 3.1.

Table 2: “Please also define  $d_s$ ,  $d_p$ , and  $L$  in the table caption”

We changed as requested:

Cumulative statistics for ATM supraglacial lakes explored in this study, including mean and maximum signal-based depth ( $d_s$ ) and polynomial-based depth ( $d_p$ ), along-track extent  $L$ , mean lake depth uncertainty...

# Using ICESat-2 and Operation IceBridge altimetry for supraglacial lake depth retrievals

Zachary Fair<sup>1</sup>, Mark Flanner<sup>1</sup>, Kelly M. Brunt<sup>2,3</sup>, Helen Amanda Fricker<sup>3</sup>, and Alex Gardner<sup>4</sup>

<sup>1</sup>University of Michigan, Ann Arbor, MI

<sup>2</sup>NASA Goddard Space Flight Center, Greenbelt, MD

<sup>3</sup>University of Maryland, College Park, MD

<sup>4</sup>Scripps Institution of Oceanography, San Diego, CA

<sup>5</sup>NASA Jet Propulsion Laboratory, Pasadena, CA

**Correspondence:** Zachary Fair (zhfair@umich.edu)

**Abstract.** Supraglacial lakes and melt ponds occur in the ablation zones of Antarctica and Greenland during the summer months. Detection of lake extent, depth, and temporal evolution is important for understanding glacier dynamics, ~~but passive remote sensing techniques have inherent uncertainties associated with depth retrievals, and observations from the original ICESat mission experienced high absorption in water.~~ Previous remote sensing observations of lake depth are limited to estimates from passive satellite imagery, which has inherent uncertainties, and there is little ground truth available. In this study, we use laser altimetry data from the Ice, Cloud, and land Elevation Satellite-2 (ICESat-2) over the Antarctic and Greenland ablation zones and the Airborne Topographic Mapper (ATM) for Hiawatha Glacier (Greenland) to demonstrate retrievals of supraglacial lake depth. Using an algorithm to separate lake surfaces and beds, we present case studies for 12 supraglacial lakes with the ATM lidar and 12 lakes with ICESat-2. Both lidars reliably detect bottom returns for lake beds as deep as 7 m. ~~Uncertainties~~ Lake bed uncertainties for these retrievals are 0.05-0.20 m for ATM and 0.12-0.80 m for ICESat-2, with the highest uncertainties observed for lakes deeper than 4 m. ~~Using ICESat-2 confidence classifications of detected photons, we found~~ The bimodal nature of lake returns means that high-confidence photons are often insufficient to fully profile lakes, so lower confidence and buffer photons are ~~recommended for improved retrievals. Despite issues in photon classification~~ required to view the lake bed. Despite challenges in automation, the altimeter results are promising, and we expect them to serve as a benchmark for future studies of surface meltwater depths.

## 1 Introduction

The ice sheets of Antarctica and Greenland modulate rates of sea level rise, contributing  $14.0 \pm 2.0$  mm (Antarctica) and  $13.7 \pm 1.1$  mm (Greenland) since 1979 (Mouginot et al., 2019; Rignot et al., 2019). Current trends indicate greater melt in the coming decades, leading to the contributions from both ice sheets ~~becoming dominant contributors to~~ to overtake the contribution of thermal expansion to sea level rise (Vaughan et al., 2013). Meltwater plays vital roles in ice sheet evolution (e.g., van den Broeke et al., 2016), including accumulation aggregation on ice sheets as supraglacial lakes, many of which are several meters deep (Echelmeyer et al., 1991). ~~These~~ When unfrozen, these lakes exhibit a lower albedo than that of the surrounding ice, allowing

them to absorb more incoming solar radiation and melt ice more efficiently, thus generating a positive feedback (Curry et al., 1996). Supraglacial lakes are significant reservoirs of latent heat (Humphrey et al., 2012), and their spectral emissivity in the IR spectrum also differs from bare ice (Chen et al., 2014; Huang et al., 2018), ~~leading which can lead~~ to potentially significant impacts on the surface energy balance of ice sheets.

5 A substantial portion of meltwater eventually drains into supraglacial streams or moulins (drainage channels), where it can flow to the ice bed (Banwell et al., 2012; Catania et al., 2008; Selmes et al., 2011). ~~Meltwater~~ During catastrophic lake drainage events, meltwater penetration into the ice ~~also leads can also lead~~ to hydrofracture, a mechanism through which meltwater facilitates full ice fracture as a result of the stresses induced by the density contrast between liquid water and ice (Das et al., 2008). Meltwater injection to the bed can also modify basal water pressures which in turn modify the resistance to  
10 ice flow and thus ~~sliding velocity can impact sliding velocity and ice discharge~~. (Parizek and Alley, 2004; Zwally et al., 2002). Hydrofracture can lead to significant ice loss for outlet glaciers and ice shelves (Banwell et al., 2013). Current observations and modeling efforts indicate a propagation of supraglacial lakes farther inland as the climate warms (Howat et al., 2013; Leeson et al., 2015; Lüthje et al., 2006), raising further concerns for accelerated mass loss. For these reasons, knowledge of supraglacial lakes is important for our understanding of ice sheet evolution.

15 Previous studies developed techniques for detecting supraglacial lakes and retrieving depth, areal coverage, and volume. In-situ observations employed sonar and radiometers to approximate lake depth and albedo (Box and Ski, 2007; Tedesco and Steiner, 2011). However, the harsh conditions of Antarctica and Greenland, the transience of meltwater, and the sheer size of the ice ~~sheets~~ sheet ablation zones restrict the potential for extensive in-situ measurements, encouraging lake depth and areal coverage estimates from passive remote sensing data such as Landsat-8, MODIS, and Sentinel-2 A/B. Supraglacial water is darker  
20 than surrounding ice in visible and IR bands, allowing the use of band ratios between blue and red reflectance (Stumpf et al., 2003). The normalized water difference index (NWDI) and dynamic thresholding techniques have also been considered for lake detection (~~Fitzpatrick et al., 2014; Liang et al., 2012; Moussavi et al., 2016; Williamson et al., 2017; Moussavi et al., 2020~~) (Fitzpatrick et al., 2014; Liang et al., 2012; Moussavi et al., 2016; Pope, 2016; Williamson et al., 2017; Moussavi et al., 2020). Other methods implemented radiative transfer models (Georgiou et al., 2009) or positive degree day models (McMillan et al.,  
25 2007) to estimate lake albedo and meltwater volume, respectively. By comparing surface reflectance data of supraglacial water to that of ice and optically deep water, empirical relationships have been derived to approximate lake depth (Philpot, 1989; Sneed and Hamilton, 2007).

Image-based empirical techniques rely on approximations of lake bed albedo and an attenuation parameter, both of which are subject to uncertainties from lake heterogeneity and cloud cover (Morassutti and Ledrew, 1996). Furthermore, Pope et al.  
30 (2016) found that band ratios were insensitive to lakes deeper than 5 m, leading to errors that may exceed 1 m. Parameter fitting in the empirical equations requires supplementary depth retrievals, often from in-situ sources. More accurate methods for supraglacial lake detection are needed to improve image-based estimates.

In September 2018, the Ice, Cloud and land Elevation Satellite-2 (ICESat-2) with the primary objective of obtaining laser altimetry measurements of the polar regions (Abdalati et al., 2010; Markus et al., 2017; Neumann et al., 2019b). Observations  
35 using the Airborne Topographic Mapper (ATM) and Multiple Altimeter Beam Experimental Lidar (MABEL) indicated the

potential for shallow water profiling with laser altimetry (Brock et al., 2002; Brunt et al., 2016; Jasinski et al., 2016), and ICESat-2 applications were recently demonstrated by Ma et al. (2019) and Parrish et al. (2019). In this study, we identify test cases from ICESat-2 and ATM altimetry data and use these pilot cases to develop an algorithm for detecting supraglacial lakes and retrieving lake depth. The algorithm is designed as a semi-automatic method to find supraglacial lakes within select  
5 altimetry granules.

## 2 Data Description

### 2.1 ICESat-2

ICESat-2 is a polar orbiting satellite with an inclination of 92 degrees that carries the Advanced Topographic Laser Altimeter System (ATLAS), a 532 nm micro-pulse laser that is split into ~~6 distinct beams~~ six distinct beams with names based on the  
10 ground track: GT1L/R, GT2L/R, and GT3L/R. The beams are configured in pairs with a 90-meter separation between beams within a beam-pair and ~~3.3-kilometer~~ kilometers between pairs. With an operational altitude of ~500 km and a 10 kHz pulse repetition rate, ICESat-2 records a unique laser pulse approximately every 0.7 m along-track over a 91-day repeat cycle.

The ATLAS product used here is the ATL03 Global Geolocated Photon Data V002 (Neumann et al., 2019a), which consists of retrieved photons tagged with latitude, longitude, received time, and elevation. Each photon pulse also carries a classification  
15 as either signal or background (noise). The differentiation between signal and background is performed using a statistical algorithm outlined by Neumann et al. (2019b). Signal photons are further classified by confidence level, such that photons labeled as "high confidence" are most likely to originate from the surface. Generally, cloudy or variable profiles exhibit "medium/low confidence" or noise photons, whereas low slope surfaces, such as water and ice sheets, result in more "high confidence" photons (Neumann et al., 2019b). In thin layers of water, high confidence photons are observed from both the water surface and  
20 the underlying ice.

~~Of the six beams available, we concentrated~~ Our study focused on the central strong beam (GT2L) ~~to increase the likelihood of detecting lake bottoms.~~, as the number of lakes was deemed sufficient for our purposes. While we recognize that the other strong beams could be useful for depth retrievals, we did not consider them here. We speculate that the weak beams may avoid issues with multiple scattering and specular reflection, but their power is too low to reliably detect lakes deeper than 4 m.  
25 Ground-based validation by Brunt et al. (2019b) indicates an accuracy of <5 cm in ATL03 photons over ice sheet interiors. ~~Only high-confidence photons were considered initially, but photons of lower confidence were included for attenuated lake bottoms (see Sect. 5.2 for more details). The addition~~ The use of medium, low, and "buffer" "buffer" photons slightly decreases measurement precision ~~but~~, but a less truncated transmit pulse gives better agreement with ATL06 and ground-based data (Brunt et al., 2019b).

## 2.2 Airborne Topographic Mapper

The ~~Airborne Topographic Mapper is a 532 nm lidar flown as part of Operation Icebridge~~ Operation IceBridge (OIB) ~~, a campaign~~ campaign was designed to fill the gap in polar altimetry between ICESat and ICESat-2. Its scientific payload included the Airborne Topographic Mapper, a 532 nm lidar that has been used for ice sheet and shallow water measurements since 1993.

5 The ATM lidar conically scans at 20 Hz, providing a 400 m swath width along-track (Brock et al., 2002; Krabill et al., 2002). The ATM Level-1B Elevation and Return Strength (ILATM1B) product converts analog waveforms into a geolocated photon elevation product to emulate ATLAS data (Studinger, 2013, updated 2018), ~~though~~. Although it lacks a statistical confidence definition, ~~Despite this,~~ ATM applies a centroid model to digitized waveforms to retrieve high-confidence photons. Brunt et al. (2019a) found that ATM errors were -9.5 to 3.6 cm relative to ground-based measurements. Currently Here, the ATM results  
10 presented serve as a proof of concept for the lake detection algorithm.

## 3 Methods

### 3.1 Lake Detection

Supraglacial lake surfaces are much flatter than surrounding terrain. We thus performed topography checks with the expectations that (i) lake surfaces would be easily-identifiable in photon histograms and (ii) lake beds may be found via statistical  
15 inference in the region of the lake surface. To simplify the identification of lake features, we separated them into two arrays: one for the surface and one for the bed. ~~We refer to this technique as "~~ which we refer to as "lake surface-bed separation" (LSBS). For both lidars, the procedure for separation was identical, and is as follows (see Fig. 2-1 for a schematic view):

- i. We divided each data granule into discrete along-track windows to reduce the data volume to  $\sim 10^4$ - $10^5$  photons per window. This photon count is equivalent to ~1-10 km in along-track distance for ICESat-2 and ~0.15-1.5 km for ATM.  
20 If a supraglacial lake appeared on the edge of the window, the window size was adjusted to include the full observed water feature.
- ii. Each data window was binned into elevation-based histograms. We assumed that the lake surface dominates the total bin count within each window of  ~~$10^5$  photons. Thus, we performed a flatness check~~ photons. We check the flatness of the window by computing the standard deviation ( $\sigma$ ) of high-confidence signal photons within the upper 85th-percentile of  
25 bin count. ~~A flatwater surface was defined for ATL03 data~~ We define a "flat" surface for regions where  $\sigma \leq 0.05$  m ~~or for ATL03 data, and  $\leq 0.002$ - $0.02$  m for ILATM1B data.~~ We selected these values by comparing the "flatness" of lake surfaces to that of surrounding ice topography. If data were within the appropriate flatness threshold, they were verified as a lake surface using Landsat-8 OLI imagery. This step was included to filter non-glacial features, such as ocean or fjords.
- 30 iii. If the satellite image(s) confirmed the presence of a lake, the data were assigned to a new array for the height of the lake surface ( ~~$h_{sfc}$~~ ).

- iv.  $h_{sfc}$ . The horizontal extent of ~~where the above criteria were met~~ the lake surface served as a constraint for where the lake bottom data could be defined. Within these horizontal bounds, ~~high-confidence~~ photons were defined as a lake bottom if they satisfied the condition:  $h_{sfc} - 1.8\sigma_{sfc} \leq h \leq h_{sfc} - 0.75\sigma_{sfc}$   ~~$h_{sfc} - a\sigma_{sfc} \leq h \leq h_{sfc} - b\sigma_{sfc}$~~ , where  $\sigma_{sfc}$  is the standard deviation of lake surface photons. ~~We set this constraint~~ The constraints  $a$  and  $b$  were derived through trial-and-error, such that  $a = 1.0(1.8)$  and  $b = 0.5(0.75)$  for ICESat-2 (ATM). We set these constraints to reduce the ~~impact~~ impacts of multiple scattering and specular reflection on depth estimates. If these conditions were met, then the data were placed in an array for the height of the lake bottom,  $h_{btm}$   $h_{btm}$ .
- v. ~~Lake bed photons often are classified at a lower confidence (Sect. 5.2), necessitating the inclusion of lower confidence levels. Notably, Greenland supraglacial lakes observed by ICESat-2 featured this issue if they exceeded 3 m in depth. For these cases, the condition for  $h_{btm}$  was revised as  $h_{sfc} - \sigma_{sfc} \leq h \leq h_{sfc} - 0.5\sigma_{sfc}$  to filter background photons within the water column.~~
- vi. A series of filters were applied to improve surface/bed estimates. For ICESat-2, lakes shallower than 1.3 m or smaller than 200 m in horizontal extent were considered too noisy or ill-defined for further analysis (see Section 5.2 for more details). To remove water bodies with deep bed returns (e.g., oceans or fjords) or with no bed returns, the algorithm counted the number of bed photons present for both lidars. If the number of bed photons was very small (100 or less), then the scene was marked as a probable false positive.
- vii. If the data were obtained from ICESat-2, then we followed a photon refinement routine that is described in more detail in Sect. 3.2. Calculations for lake depth were then performed for both ATM and ICESat-2 retrievals and corrected for refraction (Sect. 3.3).

## 20 3.2 ATL03 Refinement

The above steps were sufficient to obtain lake profiles within the ATM data, but melt lake bottoms observed by ICESat-2 were significantly noisier as a consequence of higher background (noise) photon rates. After the initial LSBS procedure, we manually assessed bed estimates for each lake. For lakes that did not pass qualitative assessment, we adopted photon refinement procedures initially used for the ATL06 surface-finding algorithm (Smith et al., 2019). In short, ATL03 photon aggregates within overlapping 40 m segments were used to estimate lake surfaces and beds with greater precision via least-squares linear fitting applied to the aggregates. These linear fits were used to approximate a window of acceptable surface or bed photons for every 20 m along-track. A more detailed description of the ATL06 algorithm is given in Smith et al. (2019).

The linear regression in ATL06 accounts for all ATL03 photons (background or signal), and the technique performs a background-corrected spread estimate to narrow the range for acceptable photons. ~~Background photons are omitted from LSBS refinement, and low-/medium-confidence photons are only considered if the high-confidence photons are deemed insufficient. The ATL06 refinement process also~~ This is an iterative scheme; the refinement process repeats its acceptable photon filter until no photons are removed. ~~In LSBS, the flatness of lake surfaces and relatively low photon density of the corresponding beds~~

~~rendered iterating unnecessary. Finally, the~~ As a consequence, the ATL06 algorithm assumes a single returning surface, so over a melt lake it will compute a height for either the lake bottom or the lake surface, depending on their return strengths.

The condition for acceptable surface photons in ATL06 is given by:

$$|r - r_{med}| < 0.5H_w \quad (1)$$

5 Within a 40 m photon segment,  $r$  is the residual of a photon relative to the linear regression,  $r_{med}$  is the median residual, and  $H_w$  is window height. The height of the window is taken as the maximum of the observed photon spread, the ~~previous~~ window height (if any) ~~, and 1 and 3 m~~, and photons within the window range are defined as the surface. The ~~lake-LSBS algorithm follows a similar procedure, but the flatness of the lake surface and relatively low photon density of the corresponding beds rendered iterating unnecessary. The lake~~ bed is then defined as photons not within the window and below the surface. In other  
10 terms, lake bed photons satisfy the conditions:

$$|r - r_{med}| > 0.5H_w, \quad h < h_{sfc} \quad (2)$$

As with the initial guess, the lake bottom was only defined within the horizontal bounds of the lake surface, and the improved guesses were assigned to  $h_{sfc}$  and  $h_{btm}$ .

As a final adjustment to lake photons, we applied a refraction correction algorithm to account for ~~spatial offsets from the~~  
15 ~~change in media~~ slowing down of light as it enters water. The correction follows the methods utilized by Parrish et al. (2019) by approximating refractive biases as a function of depth and beam elevation angle. The center strong beam for ICESat-2 is near-nadir, so the horizontal offset was determined to be small relative to the size of lakes ( $\sim 3$  cm ~~for a lake 10 m deep, far below the horizontal geolocation uncertainty for ICESat-2~~). However, vertical offsets of 1 m or more were found for lakes  $\geq 4$  m in depth, necessitating the use of refraction correction.

### 20 3.3 Lake Depth and Extent Estimations

Once we obtained  $h_{sfc}$  and  $h_{btm}$ , lake depth from the altimeter signal ( $z_s$ ) was estimated using:

$$z_s = \bar{h}_{sfc} - \bar{h}_{btm} \quad (3)$$

where  $\bar{h}_{sfc}$  and  $\bar{h}_{btm}$  represent the moving mean of the surface elevation and the bottom elevation, respectively. The moving mean was used to account for signal attenuation and scattering at the lake bottom, a problem most evident ~~over the Amery Ice~~  
25 ~~Shelf~~ for ICESat-2 retrievals.

For deep or inhomogeneous lakes, ~~water attenuation~~ attenuation of photon energy in water resulted in fewer signal photons observed at lake bottoms ~~. To approximate lake depths in~~ (Fig. 4). In these situations, we fitted ~~a 3rd-order polynomial~~ polynomial or spline fits to all lake profiles with bounds at the lake edges. Lakes observed by ATM typically featured “bowl”

shapes and attenuation at the deepest parts, so 3rd-order polynomials were sufficient. In ICESat-2 data, the retrieved lake beds showed greater complexity, so we tested polynomial fits and splines on a case-by-case basis. Lake depths approximated in this manner with curve fitting were denoted as  $z_p$ . We compare  $z_s$  and  $z_p$  over lakes with well-defined bottoms, and show in Sect. 4 that the two generally agree well, in Sect. 4 to within 0.88 m.

5 To test the limits of the algorithm relative to lake size, we utilized the great-circle formula (ATM) or pre-defined along-track distance (ICESat-2) to approximate along-track extent  $L$ . We acknowledge the further potential for lake volume retrieval, but improved estimates of lake radius and shape through visible imagery are required. We desire to retrieve lake volume from laser altimetry, but we leave the development of such an algorithm for a future study. For example, depth retrievals from ICESat-2 could potentially be combined with lake radius and shape estimations determined from visible satellite imagery to derive water  
10 volume.

### 3.4 Case Study Locations

We present cases over the Amery Ice Shelf on 2 January, 2019 (ICESat-2 Track 0081; 68.271-73.798°S, 63.057-78.620°E), the western Greenland ablation zone for 17 June, 2019 (ICESat-2 Track 1222; 66.575-69.582°N, 48.284-49.239°W), and Hiawatha Glacier in 19 July, 2017 (ATM; 77.780-79.3119°N, 65.279-67.484°W) (Fig. 42). Comparisons between Landsat-8  
15 imagery and ICESat-2/OIB flight tracks confirmed supraglacial lake overpasses for study. The tracks examined for this analysis are listed in Table 1. In Spring 2019, an early onset of the Arctic melt season resulted in both ICESat-2 and Operation Icebridge surveying supraglacial lakes near Jakobshavn Jakobshavn Isbrae in May. Data granules from ATM for this time period were not available for download. However, there were no lakes sampled at the time of publication, but we expect these observations to be useful for additional depth estimates and validation in a future study by both ICESat-2 and OIB.

## 20 4 Results

We detected a total of 16 supraglacial lakes in 12 melt lakes with sufficient bed returns from the ATM data. Of those, four were omitted from further analysis due to poor signal return from the lake bed. The remaining and 16 potential melt lake surfaces overall. The melt lake profiles are shown in Fig. 3, with maximum depths of 0.98-7.38 m and extents of 180-730 m. The algorithm identifies lake surfaces with good accuracy, and lake reliably distinguishes between lake surfaces and the surrounding ice terrain. The mean spread among lake surface photons is 0.0087 m, or well within the flatness threshold of 0.02 m. Lake bottoms are well-defined in all but the deepest lakes when  $d_s < 8$  m. Lake bottoms  $>$ deeper than 8 m below the surface exhibit fewer signal returns, for the associated return signal is below the threshold required to be digitized (Martin et al., 2012). Average measured lake depth was estimated as The average depth estimate for the lakes in Fig. 3 was 1.95 m (Table 21), and lakes at this depth typically featured adequate bed returns. In deeper lakes, the polynomial estimate produced reasonable  
25 guesses for the lake bed location, with the most effective fitting seen in lakes 3e, 3g, and 3h. With the polynomial-based depths, mean lake depth increased to 2.15 m, and the maximum modeled depth was 8.83 m.

The spread in ATM lake bed photons is low (Table 21, Column 7), with a maximum of 0.2 m for lake 3g. The ~~largest highest~~ uncertainties are observed for ~~lakes deeper lake depths greater~~ than 3 m, perhaps influenced by low ~~photon returns and signal-to-noise ratios or~~ the conical scanning of the ~~lidar OIB lidar instrument~~. Polynomial estimation errors are 0.41 m on average. Several depth errors are below this mean, but a strong standard error (1.03 m) in lake 3g, due to difficulties in capturing its steep bed slope, slightly skews the mean error. Excluding this value, the mean error among ATM polynomial estimates reduces to 0.35 m.

We examined an additional 12 supraglacial lakes with ICESat-2, eight in Greenland and four ~~also explored by Magruder et al. (2019) and Fricker et al. (in prep.)~~ on the Amery Ice Shelf ~~in Antarctica~~. ~~Three of the Antarctic melt lakes (4a, 4b, 4d) are highlighted in Magruder et al. (2019) and Fricker et al. (in prep.)~~. The refined algorithm ~~captured these captures~~ lake surfaces and beds ~~with reasonable success, as seen in Fig. 4~~, reasonably well (Fig. 4), with a mean uncertainty of 0.015 m for surface photons and 0.38 m for bed photons. ~~The lake edges partially account for the bed photon uncertainty, for the limited number of acceptable photons produces a slight bias in bed estimates~~. Antarctic melt lakes were generally shallower than those seen on Greenland (Table 32) - only lake 4a exceeded 3 m in depth, whereas the mean maximum depth over Greenland was 4.08 m. ~~The heterogeneity and noisiness of Melt lakes on the Amery Ice Shelf retrievals rendered best-fit calculations difficult and increased uncertainty estimates. However, these melt lakes~~ were 3-8 km in extent, thus facilitating detection in histograms. Greenland lakes exhibited a wider range of sizes, but the algorithm successfully performed retrievals for lakes as small as 200 m in extent.

On average, the noisier data from ICESat-2 produces uncertainties greater than 0.2 m for the Antarctic lakes and 0.3 m for the Greenland lakes, as seen in Table 32, Column 8. The inclusion of lower-confidence photons increases uncertainty despite the restricted bed photon criteria, for the larger photon cloud increases the spread of the entire lake profile. The ~~polynomial errors in ICESat-2 are comparable to ATM over Greenland, with lakes curve fits improved depth estimates for lakes 4b, 4f and 4g exhibiting notably high error. Polynomial errors are higher for the Antarctic melt ponds, as it is difficult to reproduce the complex bed topography, an observation shared with lakes~~, and 4i. Of these lakes, only 4i used a polynomial estimate due to ~~poor spline fitting. The inclusion of interpolants increased the mean depth estimates of 4b, 4f and 4g from Greenland. It also must be noted that bed photons are more likely to be found in the ATL03 photon cloud than in ATM waveforms, and 4i by 0.08 m, 0.04 m, and 0.03 m, respectively. The spline fitting significantly increased the maximum observed depth in lake 4b from 2.67 m to 3.27 m. The remaining lakes featured more complete bed profiles~~, meaning that the ~~polynomial estimates are less necessary for ICESat-2 than when used for ATM fitting estimates were less important~~.

## 5 Discussion

### 5.1 Algorithm Performance

The conical scanning of the ATM lidar produced oscillations in 1D elevation profiles that dampened over lake surfaces, so lakes generally were easier to identify with the airborne retrievals. Flights conducted during the OIB campaign actively avoided cloudy conditions, reducing attenuation sources and further simplifying the lake-finding process over common melt regions. The data volume per granule was lower than ATL03, resulting in less time needed to run the algorithm. However, the number

of retrievals possible with ATM is limited, so observations with the lidar best serve as a validation and correction tool for ICESat-2 and other retrieval methods.

The laser power and detector sensitivity of the ATLAS instrument on board ICESat-2 are sufficient to reliably detect lake beds, and a high along-track resolution will correspond to improved estimates of lake bed topography, water depth, and water volume. Despite strong advantages, significant difficulties must be considered before automatic lake detection is feasible. At its operational altitude, the ATLAS laser is subject to first-photon-bias, solar background radiation, and scattering and absorption by blowing snow and clouds. Clouds are common over the fringes of Antarctica and Greenland (Bennartz et al., 2013; Lachlan-Cope, 2010; Van Tricht et al., 2016), and often their optical depth is sufficient to render the surface undetectable. Handling the large data volumes in ATL03 granules also presents a significant challenge. A single granule provides coverage over hundreds of kilometers, so the running time of the algorithm increases relative to ATM granules. Lakes smaller than 1 km are difficult to automatically detect with the algorithm, but LSBS may still be performed for lakes as small as 200 m if the location of a lake is known through other means (e.g., Landsat-8 imagery or ATM retrievals).

We ~~attribute~~ observed differences in lake topography for ICESat-2 lakes, and we attribute them to the underlying ice surfaces. Supraglacial lakes on Greenland typically form into smooth basins within depressions formed by the underlying bedrock, and their location is independent of ice motion (Echelmeyer et al., 1991). In contrast, meltwater on the Amery Ice Shelf originates from the blue ice zone, propagating along the ice surface in streams. The location of lakes and ice topography are thus tied to the flowlines of the ice shelf surface. These features are flooded in the Antarctic melt season, producing melt lakes and streams up to 80 km in length (Mellor and McKinnon, 1960; Phillips, 1998; Kingslake et al., 2017).

## 5.2 ~~ATL03 Photon Classification Uncertainties~~

~~The classification of ATL03 signal photons provides challenges for automatic depth retrievals. The signal confidence for photons is provided through the~~ A potential issue for lake depth retrievals concerns specular reflection. When photons interact with a flat water surface, they may reflect directly back to the detector with minimal energy loss. The excessive return energy produces a “signal\_conf\_phdead\_time” variable, with higher values (at a maximum of 4) indicating greater confidence that a photon is the signal in the ATLAS detector, and the return signal is represented by multiple subsurface returns below the actual surface (Neumann et al., 2020). An example of this phenomenon may be seen in Fig. 4f, where a prominent subsurface return 1 m below the true surface is featured along the lake extent. However, ~~the confidence variable is given as a 5 x N matrix, where each row represents a surface type (land, ice, inland water, etc.). The confidence level for photons varies between surface types (Neumann et al., 2019b), and photons may be assigned to multiple surface types. Furthermore, the water masks used for surface classification do not factor melt lakes because the subsurface echo is smaller than the true surface when viewed through~~ histograms, the LSBS algorithm is able to avoid biases caused by specular reflection.

The success of this method for lake depth retrievals is governed by spatial and temporal sampling of the instruments across the lakes when they are full. The methods presented here are most effective when the altimeter passes directly over the deep part of a lake rather than at its edge. This provides a lake depth profile that is more representative of the complete lake, allowing for improved estimates of lake depth and extent. A complete lake profile also provides sufficient information to the LSBS

algorithm, reducing the risk of false negatives that occur with small lakes or incomplete profiles. The temporal sampling of ICESat-2 and ATM is infrequent (every 91-days for ICESat-2 and random for ATM), and so the same lakes will not always be present every time these data are required. Therefore, coincident satellite imagery is desirable to simplify the lake-finding process.

## 5 5.2 Automation Challenges

The identification of lake beds in the LSBS algorithm is based on a window of acceptable photons. The photon window is constrained by the coefficients  $a$  and  $b$  (for ICESat-2, ~~so lakes on ice sheet surfaces are not identified. Instead, lake surfaces in ATL03 typically classify as "land ice", and lake beds as either "land ice" or "land"~~  $a = 1.0$ ,  $b = 0.5$ ). Lake beds detected in this manner had a height uncertainty of 0.38 m (Table 2). The coefficients for ATM ( $a = 1.8$ ,  $b = 0.75$ ), resulted in more accurate retrievals on an individual basis. However, implementing varying  $a$  and  $b$  values proved difficult to automate, as other values may produce more accurate depths.

The ~~example in Fig. 5 shows the differences between the two surface types. The land-only photons identify the lake surface and portions of the lake bed with high confidence, whereas the lake bed exhibits lower confidence in the land ice classification. For lake beds, photons >2 m below the surface are more likely to be assigned the~~ challenges in full automation are related to three key issues. First, the observed extent of lakes varied considerably, especially over Greenland. The diversity in lake sizes complicated attempts to derive a universal "landflatness" classification. ~~We theorize this occurs because the lake resembles a tree canopy in 1-D profiles. To circumvent this issue, the LSBS algorithm includes a routine that takes the highest confidence level among all surface types for each photon in a data granule. check.~~ Smaller lakes present fewer lake surface photons, so a smaller data window ( $\sim 10^4$  photons) is required to prevent false positives. However, larger lakes may not be fully represented in smaller windows. A larger data window ( $\sim 10^5$  photons) will fully capture the largest lakes, but smaller lakes may then be overlooked.

~~By default, the LSBS algorithm incorporates high-/medium-/low-confidence signal photons~~ Second, multiple scattering at the lake bed increases the photon spread and thus also increases the uncertainty of depth retrievals. Most supraglacial lakes observed by ATM featured smooth beds, so photons experienced one or few scattering events before returning to the detector. The instrument digitizer automatically filters return signals with low photon counts, reducing the spread of bed photons, at the cost of deep lake bottom detection. In contrast, the lakes observed with ICESat-2 exhibited more heterogeneous beds, leading to increased scattering events by photons and delays in return pulses. In these cases, the given values for  $a$  and "buffer" photons  $b$  may not produce the most accurate bed solution. Furthermore, if the return is significant for a given photon window, then it may lead to a false negative for a portion of the lake (Figure 4i). To reduce uncertainty in lake depth retrievals, future improvements in working with ICESat-2 data should focus on identifying and filtering multiple scattering. ~~This approach is necessary for most melt lakes observed by ICESat-2, as lake beds frequently receive lower confidence flags. For instance, melt lake 4a features an incomplete bed when only high confidence photons are considered. The~~

Finally, the ATL03 signal-finding algorithm is conservative in that it accepts false positives (background photons classified as signal photons) to ensure that all signal photons are passed to higher-level products. Thus, uncertainties in the ATL03

photon classification contribute to noise in the water column and the lake bed. The classification algorithm uses pre-defined surface masks to allocate statistical confidence to ATL03 photons for multiple surface types (e.g. “inland water”, “land ice”, “land”), with overlap possible between masks (Neumann et al., 2020). Melt lakes are categorized as “land ice” (lake surface) and “land” (lake surface and bed). Because the “land” classification also includes the bed, it includes more potential signal photons than *land ice*, so our recommendation is to only use *land* photons for supraglacial lake depth retrievals. It must be noted, however, that a lake bed profile is fully resolved only with the inclusion of low-/medium- confidence and “buffer” photons reveals a complete bed profile, increasing the maximum depth estimate from 2.60 m to 4.57 m, as seen in Fig. 5a. Thus, it is recommended to include photons of multiple confidence levels, otherwise the lake bed may appear attenuated and hinder retrieval efforts. The buffer photons ensure that all photons identified as surface signal are provided to the appropriate upper-level data product algorithms. However, they can introduce greater noise to the profile, so more sophisticated filtering techniques are needed to distinguish between signal photons and the solar background.

## 6 Conclusions

We present a method to detect supraglacial lakes and estimate lake depth from 532 nm laser altimetry data. We establish test cases for lake detection over two regions of Greenland (Hiawatha Glacier, 19 July, 2017 and Jakobshavn-Jakobshavn Isbræ, 17 June, 2019) and East Antarctica (Amery Ice Shelf, 2 January, 2019), and our results demonstrate that depth retrievals are possible using laser altimetry. Verification of lake detection is given with lake surface flatness tests, where we observe low topographical variance over lake surfaces relative to surrounding ice. Lake bottoms are easy to identify once lake surfaces are established, given that the lakes are not too deep deeper than 7 m.

We introduce lake a surface-bed separation scheme for ATM and ICESat-2 geolocated photon data to determine the maximum depth of lakes. Our results indicate that altimetry signals reliably detect bottoms as deep as 7 m, after which absorption of the photons in water reduces the number of reflected photons. Heterogeneity at the lake bed also produces attenuation, complicating retrieval attempts for lakes with rough bed topography or with high impurity concentration. Additional work is required to assess the impacts of lake impurities and geometry on altimetry signals and to improve estimates for such cases. Despite these shortcomings, we anticipate retrieval capability to improve as observations from the 2019 and 2020 Arctic melt seasons are released.

We establish the feasibility for estimates of supraglacial lake depth over Antarctica and Greenland. The high accuracy of 532 nm laser altimeters allow these results to serve as a benchmark for future retrieval studies. Future studies need to examine the accuracy of ICESat-2 lake retrievals relative to ATM where applicable, with additional comparisons to depth estimates from passive imaging sensors.

*Code and data availability.* ICESat-2 ATL03 V002 and ATM L1B V002 data may be accessed from <https://doi.org/10.5067/ATLAS/ATL03.002> and <https://doi.org/10.5067/19SIM5TXKPGT>, respectively. Depth data for lakes in Figure 3 are available upon request from Zachary Fair.

Depth data for the supraglacial lakes given in Figure 4 are available at <https://doi.org/10.5281/zenodo.3838274>. The LSBS algorithm and its subroutines may also be accessed from <https://doi.org/10.5281/zenodo.3838274>.

*Competing interests.* The authors declare that they have no conflict of interest.

## References

- Abdalati, W., Zwally, H. J., Bindenschadler, R., Csatho, B., Farrell, S. L., Fricker, H. A., Harding, D., Kwok, R., Lefsky, M., Markus, T., Marshak, A., Neumann, T., Palm, S., Schutz, B., Smith, B., Spinhirne, J., and Webb, C.: The ICESat-2 Laser Altimetry Mission, Proceedings of the IEEE, 98, 735–751, <https://doi.org/10.1109/JPROC.2009.2034765>, 2010.
- 5 Banwell, A. F., Arnold, N. S., Willis, I. C., Tedesco, M., and Ahlstrøm, A. P.: Modeling supraglacial water routing and lake filling on the Greenland Ice Sheet, *Journal of Geophysical Research: Earth Surface*, 117, <https://doi.org/10.1029/2012JF002393>, 2012.
- Banwell, A. F., MacAyeal, D. R., and Sergienko, O. V.: Breakup of the Larsen B Ice Shelf triggered by chain reaction drainage of supraglacial lakes, *Geophysical Research Letters*, 40, 5872–5876, <https://doi.org/10.1002/2013GL057694>, 2013.
- Bennartz, R., Shupe, M. D., Turner, D. D., Walden, V. P., Steffen, K., Cox, C. J., Kulie, M. S., Miller, N. B., and Petterson, C.: July 2012  
10 Greenland melt extent enhanced by low-level liquid clouds, *Nature*, 496, 83–86, <https://doi.org/10.1038/nature12002>, 2013.
- Box, J. E. and Ski, K.: Remote sounding of Greenland supraglacial melt lakes: implications for subglacial hydraulics, *Journal of Glaciology*, 53, 257–265, <https://doi.org/10.3189/172756507782202883>, 2007.
- Brock, J. C., Wright, C. W., Sallenger, A. H., Krabill, W., and Swift, R.: Basis and Methods of NASA Airborne Topographic Mapper Lidar Surveys for Coastal Studies, *Journal of Coastal Research*, 18, 1–13, 2002.
- 15 Brunt, K. M., Neumann, T. A., Amundson, J. M., Kavanaugh, J. L., Moussavi, M. S., Walsh, K. M., Cook, W. B., and Markus, T.: MABEL photon-counting laser altimetry data in Alaska for ICESat-2 simulations and development, *The Cryosphere*, 10, 1707–1719, <https://doi.org/10.5194/tc-10-1707-2016>, 2016.
- Brunt, K. M., Neumann, T. A., and Larsen, C. F.: Assessment of altimetry using ground-based GPS data from the 88S Traverse, Antarctica, in support of ICESat-2, *The Cryosphere*, 13, 579–590, <https://doi.org/https://doi.org/10.5194/tc-13-579-2019>, 2019a.
- 20 Brunt, K. M., Neumann, T. A., and Smith, B. E.: Assessment of ICESat-2 Ice Sheet Surface Heights, Based on Comparisons Over the Interior of the Antarctic Ice Sheet, *Geophysical Research Letters*, 46, 13 072–13 078, <https://doi.org/10.1029/2019GL084886>, 2019b.
- Catania, G. A., Neumann, T. A., and Price, S. F.: Characterizing englacial drainage in the ablation zone of the Greenland ice sheet, *Journal of Glaciology*, 54, 567–578, <https://doi.org/10.3189/002214308786570854>, 2008.
- Chen, X., Huang, X., and Flanner, M. G.: Sensitivity of modeled far-IR radiation budgets in polar continents to treatments of snow surface  
25 and ice cloud radiative properties, *Geophysical Research Letters*, 41, 6530–6537, <https://doi.org/10.1002/2014GL061216>, 2014.
- Curry, J. A., Rossow, W. B., Randall, D., and Schramm, J. L.: Overview of Arctic Cloud and Radiation Characteristics, *Journal of Climate*, 9, 1731–1764, 1996.
- Das, S. B., Joughin, I., Behn, M. D., Howat, I. M., King, M. A., Lizarralde, D., and Bhatia, M. P.: Fracture Propagation to the Base of the Greenland Ice Sheet During Supraglacial Lake Drainage, *Science*, 320, 778–781, <https://doi.org/10.1126/science.1153360>, 2008.
- 30 Echelmeyer, K., Clarke, T. S., and Harrison, W. D.: Surficial glaciology of Jakobshavns Isbrae, West Greenland: Part I. Surface morphology, *Journal of Glaciology*, 37, 368–382, 1991.
- Fitzpatrick, A. A. W., Hubbard, A. L., Box, J. E., Quincey, D. J., van As, D., Mikkelsen, A. P. B., Doyle, S. H., Dow, C. F., Hasholt, B., and Jones, G. A.: A decade (2002–2012) of supraglacial lake volume estimates across Russell Glacier, West Greenland, *The Cryosphere*, 8, 107–121, <https://doi.org/10.5194/tc-8-107-2014>, 2014.
- 35 Fricker, H. A., Arndt, P., Adusumilli, S., Brunt, K. M., Datta, T., Fair, Z., Jasinski, M., Kingslake, J., Magruder, L., Moussavi, M., Pope, A., and Spergel, J. J.: Revisiting surface meltstreams on Amery Ice Shelf, East Antarctica, in prep.

- Georgiou, S., Shepherd, A., McMillan, M., and Nienow, P.: Seasonal evolution of supraglacial lake volume from ASTER imagery, *Annals of Glaciology*, 50, 95–100, <https://doi.org/10.3189/172756409789624328>, 2009.
- Howat, I. M., de la Peña, S., van Angelen, J. H., Lenaerts, J. T. M., and van den Broeke, M. R.: Brief Communication: Expansion of meltwater lakes on the Greenland Ice Sheet, *The Cryosphere*, 7, 201–204, <https://doi.org/10.5194/tc-7-201-2013>, 2013.
- 5 Huang, X., Chen, X., Flanner, M., Yang, P., Feldman, D., and Kuo, C.: Improved Representation of Surface Spectral Emissivity in a Global Climate Model and Its Impact on Simulated Climate, *Journal of Climate*, 31, 3711–3727, <https://doi.org/10.1175/JCLI-D-17-0125.1>, 2018.
- Humphrey, N. F., Harper, J. T., and Pfeffer, W. T.: Thermal tracking of meltwater retention in Greenland’s accumulation area, *Journal of Geophysical Research: Earth Surface*, 117, <https://doi.org/10.1029/2011JF002083>, 2012.
- Jasinski, M. F., Stoll, J. D., Cook, W. B., Ondrusek, M., Stengel, E., and Brunt, K.: Inland and near-shore water profiles derived from the high-altitude Multiple Altimeter Beam Experimental Lidar (MABEL), *J. Coast. Res.*, 76, 44–55, 2016.
- 10 Kingslake, J., Ely, J. C., Das, I., and Bell, R. E.: Widespread movement of meltwater onto and across Antarctic ice shelves, *Nature*, 544, 349–352, <https://doi.org/10.1038/nature22049>, 2017.
- Krabill, W., Abdalati, W., Frederick, E., Manizade, S., Martin, C., Sonntag, J., Swift, R., Thomas, R., and Yungel, J.: Aircraft laser altimetry measurement of elevation changes of the greenland ice sheet: technique and accuracy assessment, *Journal of Geodynamics*, 34, 357–376, [https://doi.org/10.1016/S0264-3707\(02\)00040-6](https://doi.org/10.1016/S0264-3707(02)00040-6), 2002.
- 15 Lachlan-Cope, T.: Antarctic clouds, *Polar Research*, 29, 150–158, <https://doi.org/10.3402/polar.v29i2.6065>, 2010.
- Leeson, A. A., Shepherd, A., Briggs, K., Howat, I., Fettweis, X., Morlighem, M., and Rignot, E.: Supraglacial lakes on the Greenland ice sheet advance inland under warming climate, *Nature Climate Change*, 5, 51–55, <https://doi.org/10.1038/nclimate2463>, 2015.
- Liang, Y.-L., Colgan, W., Lv, Q., Steffen, K., Abdalati, W., Stroeve, J., Gallaher, D., and Bayou, N.: A decadal investigation of supraglacial lakes in West Greenland using a fully automatic detection and tracking algorithm, *Remote Sensing of Environment*, 123, 127–138, <https://doi.org/10.1016/j.rse.2012.03.020>, 2012.
- 20 Lüthje, M., Pedersen, L., Reeh, N., and Greuell, W.: Modelling the evolution of supraglacial lakes on the West Greenland ice-sheet margin, *Journal of Glaciology*, 52, 608–618, <https://doi.org/10.3189/172756506781828386>, 2006.
- Ma, Y., Xu, N., Sun, J., Wang, X. H., Yang, F., and Li, S.: Estimating water levels and volumes of lakes dated back to the 1980s using Landsat imagery and photon-counting lidar datasets, *Remote Sensing of Environment*, 232, 111–128, <https://doi.org/10.1016/j.rse.2019.111287>, 2019.
- 25 Magruder, M., Fricker, H. A., Farrell, S. L., Brunt, K. M., Gardner, A., Hancock, D., Harbeck, K., Jasinski, M., Kwok, R., Kurtz, N., Lee, J., Markus, T., Morison, J., Neuenschwander, A., Palm, S., Popescu, S., Smith, B., and Yang, Y.: New Earth orbiter provides a sharper look at a changing planet, *Eos*, 100, <https://doi.org/10.1029/2019EO133233>, 2019.
- 30 Markus, T., Neumann, T., Martino, A., Abdalati, W., Brunt, K., Csatho, B., Farrell, S., Fricker, H., Gardner, A., Harding, D., Jasinski, M., Kwok, R., Magruder, L., Lubin, D., Luthcke, S., Morison, J., Nelson, R., Neuenschwander, A., Palm, S., Popescu, S., Shum, C., Schutz, B. E., Smith, B., Yang, Y., and Zwally, J.: The Ice, Cloud, and land Elevation Satellite-2 (ICESat-2): Science requirements, concept, and implementation, *Remote Sensing of Environment*, 190, 260–273, <https://doi.org/10.1016/j.rse.2016.12.029>, 2017.
- Martin, C. F., Krabill, W. B., Manizade, S. S., Russel, R. L., Sonntag, J. G., Swift, R. N., and Yungel, J. K.: Airborne Topographic Mapper Calibration Procedures and Accuracy Assessment, Tech. Rep. 215891, NASA Goddard Space Flight Center, <https://ntrs.nasa.gov/archive/nasa/casi.ntrs.nasa.gov/20120008479.pdf>, 2012.
- 35 McMillan, M., Nienow, P., Shepherd, A., Benham, T., and Sole, A.: Seasonal evolution of supra-glacial lakes on the Greenland Ice Sheet, *Earth and Planetary Science Letters*, 262, 484–492, <https://doi.org/10.1016/j.epsl.2007.08.002>, 2007.

- Mellor, M. and McKinnon, G.: The Amery Ice Shelf and its hinterland, *Polar Record*, 10, 30–34, <https://doi.org/10.1017/S0032247400050579>, 1960.
- Morassutti, M. P. and Ledrew, E. F.: Albedo and depth of melt ponds on sea-ice, *International Journal of Climatology*, 16, 817–838, [https://doi.org/http://doi.wiley.com/10.1002/\(SICI\)1097-0088\(199607\)](https://doi.org/http://doi.wiley.com/10.1002/(SICI)1097-0088(199607)), 1996.
- 5 Mouginot, J., Rignot, E., Bjørk, A., van den Broeke, M., Millan, R., Morlighem, M., Noël, B., Scheuchl, B., and Wood, M.: Forty-six years of Greenland Ice Sheet mass balance from 1972 to 2018, *Proceedings of the National Academy of Sciences*, 116, 9239–9244, <https://doi.org/https://doi.org/10.1073/pnas.1904242116>, 2019.
- Moussavi, M., Pope, A., Halberstadt, A. R. W., D., T. L., Cioffi, L., and Abdalati, W.: Antarctic Supraglacial Lake Detection Using Landsat 8 and Sentinel-2 Imagery: Towards Continental Generation of Lake Volumes, *Remote Sensing*, 12, <https://doi.org/2072-4292/12/1/134>,  
10 2020.
- Moussavi, M. S., Abdalati, W., Pope, A., Scambos, T., Tedesco, M., MacFerrin, M., and Grigsby, S.: Derivation and validation of supraglacial lake volumes on the Greenland Ice Sheet from high-resolution satellite imagery, *Remote Sensing of Environment*, 183, 294–303, <https://doi.org/10.1016/j.rse.2016.05.024>, 2016.
- Neumann, T., Brenner, A., Hancock, D., Robbins, J., Saba, J., Harbeck, K., Gibbons, A., Lee, J., Luthcke, S., and Rebold, T.: Ice, Clouds,  
15 and Land Elevation Satellite-2 (ICESat-2): Algorithm Theoretical Basis Document (ATBD) for Geolocated Photons, Tech. rep., NASA Goddard Space Flight Center, [https://icesat-2.gsfc.nasa.gov/sites/default/files/u71/ICESat2\\_ATL03\\_ATBD\\_r003\\_v2.pdf](https://icesat-2.gsfc.nasa.gov/sites/default/files/u71/ICESat2_ATL03_ATBD_r003_v2.pdf), 2020.
- Neumann, T. A., Brenner, A., Hancock, D., Robbins, J., Luthcke, S. B., Harbeck, K., Lee, J., Gibbons, A., Saba, J., and Brunt, K.: ATLAS/ICESat-2 L2A Global Geolocated Photon Data, Version 2, <https://doi.org/10.5067/ATLAS/ATL03.001>, accessed: 2019-07-19, 2019a.
- 20 Neumann, T. A., Martino, A. J., Markus, T., Bae, S., Bock, M. R., Brenner, A. C., Brunt, K. M., Cavanaugh, J., Fernandes, S. T., Hancock, D. W., Harbeck, K., Lee, J., Kurtz, N. T., Luers, P. J., Luthcke, S. B., Margruder, L., A., P. T., Ramos-Izquierdo, L., Rebold, T., Skoog, J., and Thomas, T. C.: The Ice, Clouds and Land Elevation Satellite-2 mission: A global geolocated photon product derived from the Advanced Topographic Laser Altimeter System, *Remote Sensing of Environment*, 233, <https://doi.org/https://doi.org/10.1016/j.rse.2019.111325>, 2019b.
- 25 Parizek, B. R. and Alley, R. B.: Implications of increased Greenland surface melt under global-warming scenarios: ice-sheet simulations, *Quaternary Science Reviews*, 23, 1013–1027, 2004.
- Parrish, C. E., Magruder, L. A., Neuenschwander, A. L., Forfinski-Sarkozi, N., Alonzo, M., and Jasinki, M.: Validation of ICESat-2 ATLAS bathymetry and analysis of ATLAS’s bathymetric mapping performance, *Remote Sensing*, 11, 1634, <https://doi.org/10.3390/rs11141634>, 2019.
- 30 Phillips, H. A.: Surface meltstreams on the Amery Ice Shelf, East Antarctica, *Annals of Glaciology*, 27, 177–181, 1998.
- Philpot, W. D.: Bathymetric mapping with passive multispectral imagery, *Applied Optics*, 28, 1569–1578, <https://doi.org/10.1364/AO.28.001569>, 1989.
- Pope, A.: Reproducibly estimating and evaluating supraglacial lake depth with Landsat 8 and other multispectral sensors, *Earth and Space Science*, 3, 176–188, <https://doi.org/10.1002/2015EA000125>, 2016.
- 35 Pope, A., Scambos, T. A., Moussavi, M., Tedesco, M., Willis, M., Shean, D., and Grigsby, S.: Estimating supraglacial lake depth in West Greenland using Landsat 8 and comparison with other multispectral methods, *The Cryosphere*, 10, 15–27, <https://doi.org/10.5194/tc-10-15-2016>, 2016.

- Rignot, E., Mouginot, J., Scheuchl, B., van den Broeke, M., van Wessem, M. J., and Morlighem, M.: Four decades of Antarctic Ice Sheet mass balance from 1979–2017, *Proceedings of the National Academy of Sciences*, 116, 1095–1103, <https://doi.org/10.1073/pnas.1812883116>, 2019.
- Selmes, N., Murray, T., and James, T. D.: Fast draining lakes on the Greenland Ice Sheet, *Geophysical Research Letters*, 38, <https://doi.org/10.1029/2011GL047872>, 2011.
- Smith, B., Fricker, H., Holschuh, N., Gardner, A. S., Adusumilli, S., Brunt, K. M., Csatho, B., Harbeck, K., Huth, A., Neumann, T., Nilsson, J., and Siegfried, M.: Land ice height-retrieval algorithm for NASA's ICESat-2 photon-counting laser altimeter, *Remote Sensing of Environment*, 233, 111 352, <https://doi.org/10.1016/j.rse.2019.111352>, 2019.
- Sneed, W. A. and Hamilton, G. S.: Evolution of melt pond volume on the surface of the Greenland Ice Sheet, *Geophysical Research Letters*, 34, <https://doi.org/10.1029/2006GL028697>, 2007.
- Studinger, M.: IceBridge ATM L1B Elevation and Return Strength, Version 2, <https://doi.org/10.5067/19SIM5TXKPGT>, accessed: 2018-07-14, 2013, updated 2018.
- Stumpf, R. P., Holderied, K., and Sinclair, M.: Determination of water depth with high-resolution satellite imagery over variable bottom types, *Limnology and Oceanography*, 48, 547–556, [https://doi.org/10.4319/lo.2003.48.1\\_part\\_2.0547](https://doi.org/10.4319/lo.2003.48.1_part_2.0547), 2003.
- Tedesco, M. and Steiner, N.: In-situ multispectral and bathymetric measurements over a supraglacial lake in western Greenland using a remotely controlled watercraft, *The Cryosphere*, 5, 445–452, <https://doi.org/10.5194/tc-5-445-2011>, 2011.
- van den Broeke, M. R., Enderlin, E. M., Howat, I. M., Munneke, P. K., Noel, B. P. Y., van de Berg, W. J., van Meijgaard, E., and Wouters, B.: On the recent contribution of the Greenland ice sheet to sea level change, *The Cryosphere*, 10, 1933–1946, <https://doi.org/10.5194/tc-10-1933-2016>, 2016.
- Van Tricht, K., Lhermitte, S., Lenaerts, J. T. M., Gorodetskaya, I. V., L'Ecuyer, T. S., Noël, B., van den Broeke, M. R., Turner, D. D., and van Lipzig, N. P. M.: Clouds enhance Greenland ice sheet meltwater runoff, *Nature Communications*, 7, <https://doi.org/10.1038/ncomms10266>, 2016.
- Vaughan, D., Comiso, J., Allison, I., Carrasco, J., Kaser, G., Kwok, R., Mote, P., Murray, T., Paul, F., Ren, J., Rignot, E., Solomina, O., Steffen, K., and Zhang, T.: Chapter 4: Observations: Cryosphere, Tech. rep., IPCC AR5 WG1, 2013.
- Williamson, A. G., Arnold, N. S., Banwell, A. F., and Willis, I. C.: A Fully Automated Supraglacial lake area and volume Tracking (“FAST”) algorithm: Development and application using MODIS imagery of West Greenland, *Remote Sensing of Environment*, 196, 113–133, <https://doi.org/10.1016/j.rse.2017.04.032>, 2017.
- Zwally, H. J., Abdalati, W., Herring, T., Larson, K., Saba, J., and Steffen, K.: Surface Melt-Induced Acceleration of Greenland Ice-Sheet Flow, *Science*, 297, 218–222, <https://doi.org/10.1126/science.1072708>, 2002.

True-color Landsat-8 composites of Hiawatha Glacier on 18 July, 2017 (a), the Amery Ice Shelf on 1 January, 2019 (b), and the western Greenland ablation zone on 17 June, 2019 (c). Flight tracks for Operation IceBridge (a) and ICESat-2 (b, c) are shown in dotted orange.

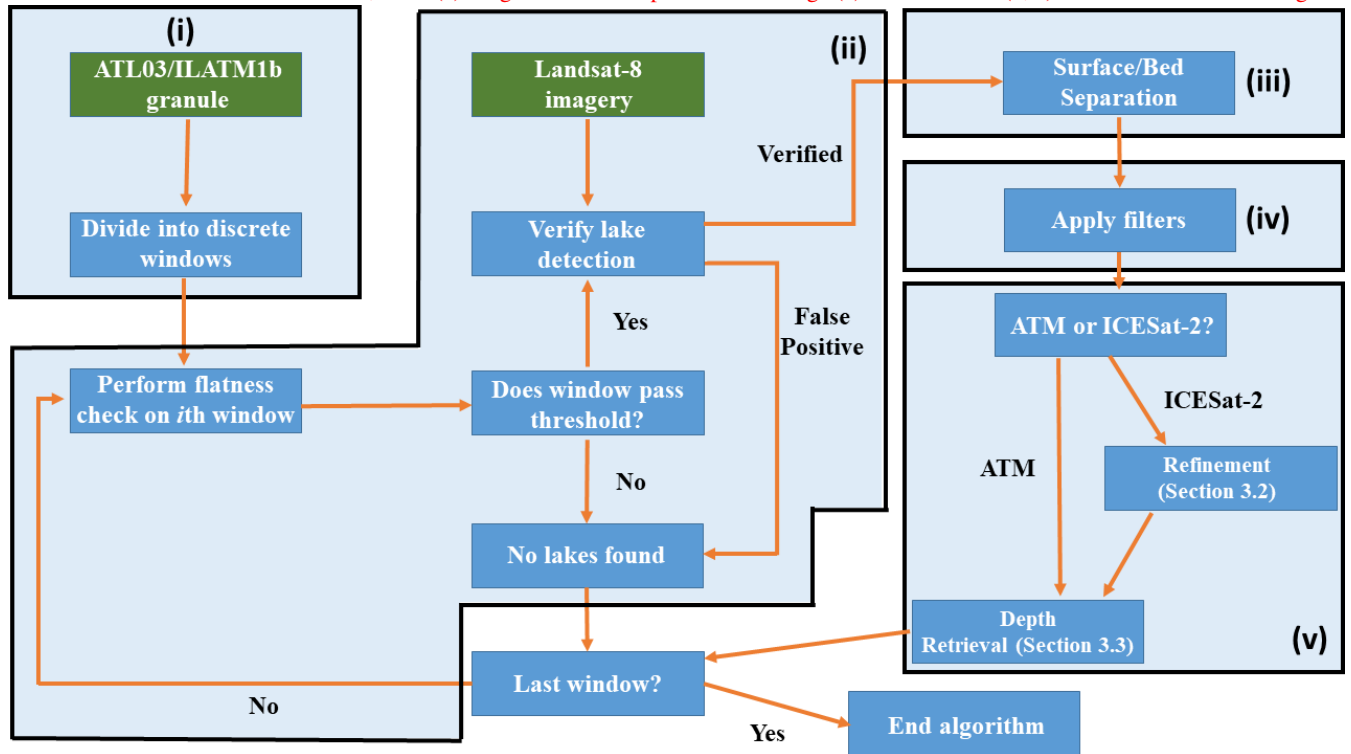
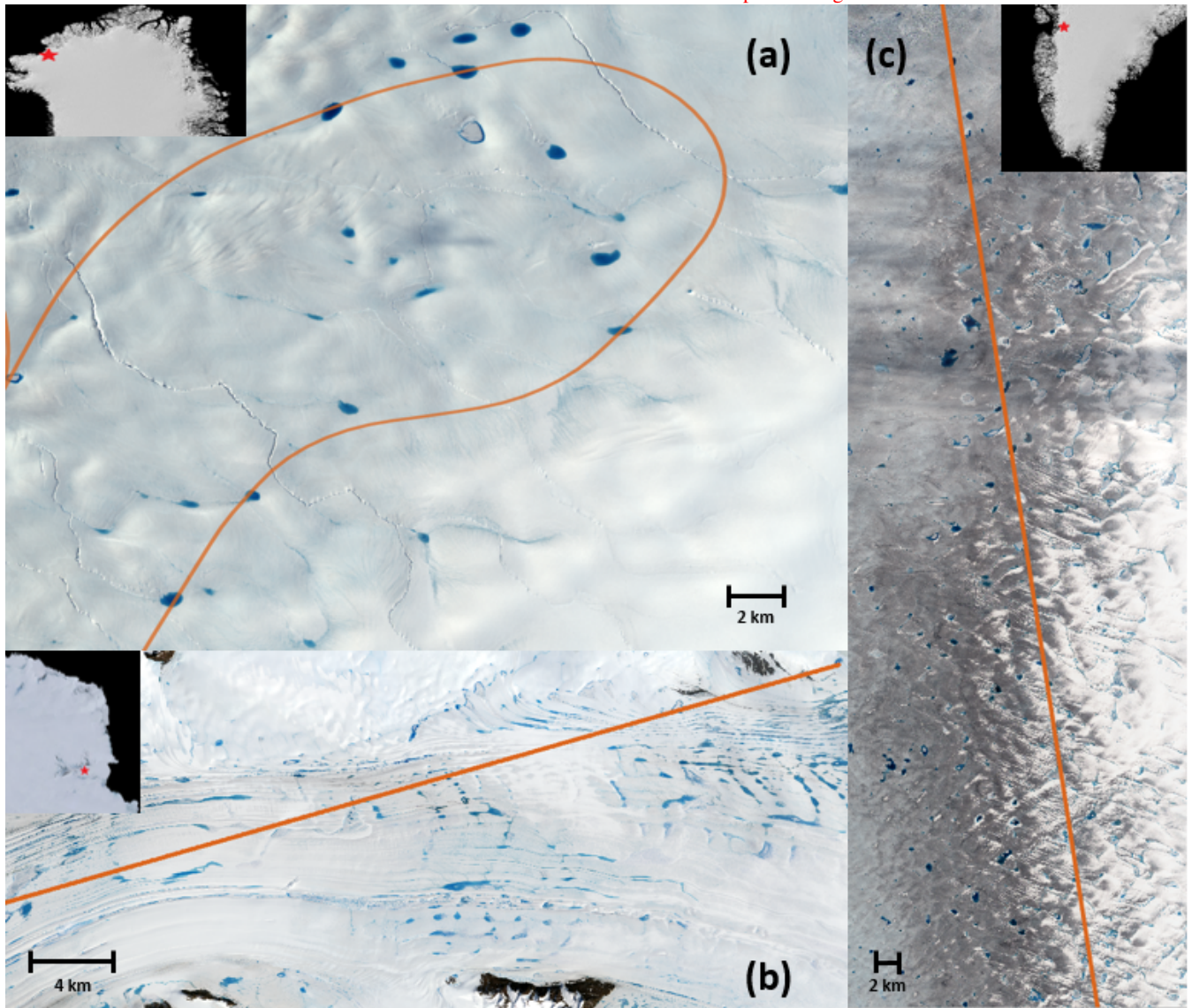
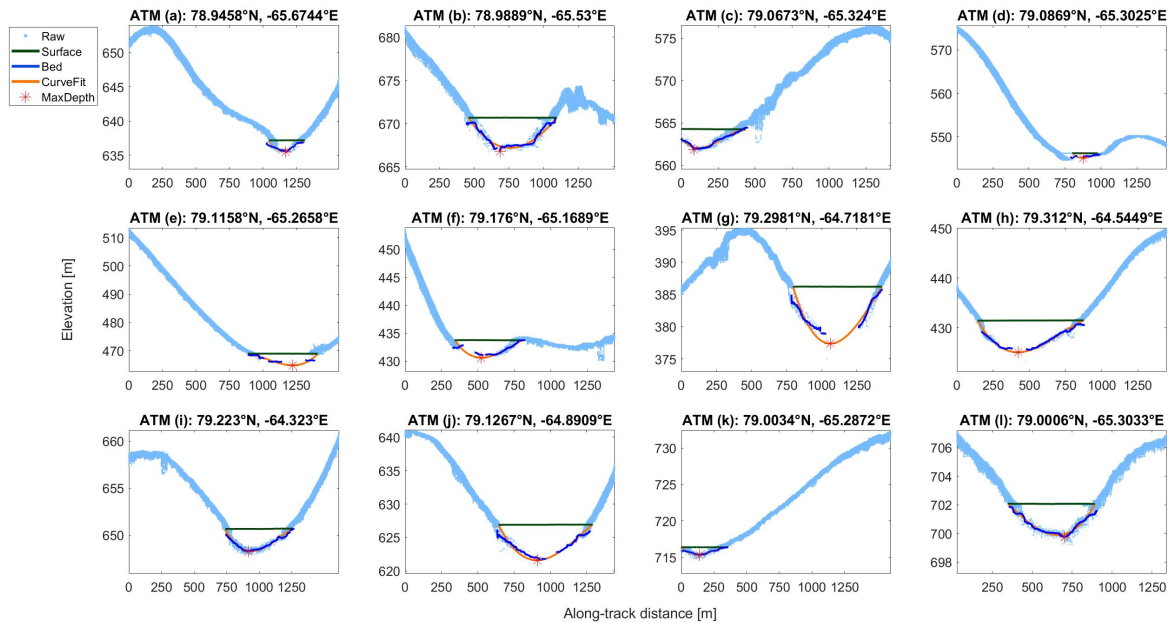


Figure 1. Schematic for the workflow of the lake surface-bed separation algorithm.

Schematic for the workflow of the lake surface-bed separation algorithm.



**Figure 2.** True-color Landsat-8 composites of Hiawatha Glacier on 18 July, 2017 (a), the Amery Ice Shelf on 1 January, 2019 (b), and the western Greenland ablation zone on 17 June, 2019 (c). Flight tracks for Operation IceBridge (a) and ICESat-2 (b, c) are shown in dotted orange.



**Figure 3.** ATM lake profiles from 17 July, 2017 fitted using lake surface-bed separation, including the raw ILATM1B product, the lake surface signal, the lake bottom signal, the polynomial-fitted polynomial-/spline-fitted bottom, and the point of maximum depth. Along-track distance is relative to the start of a data granule.

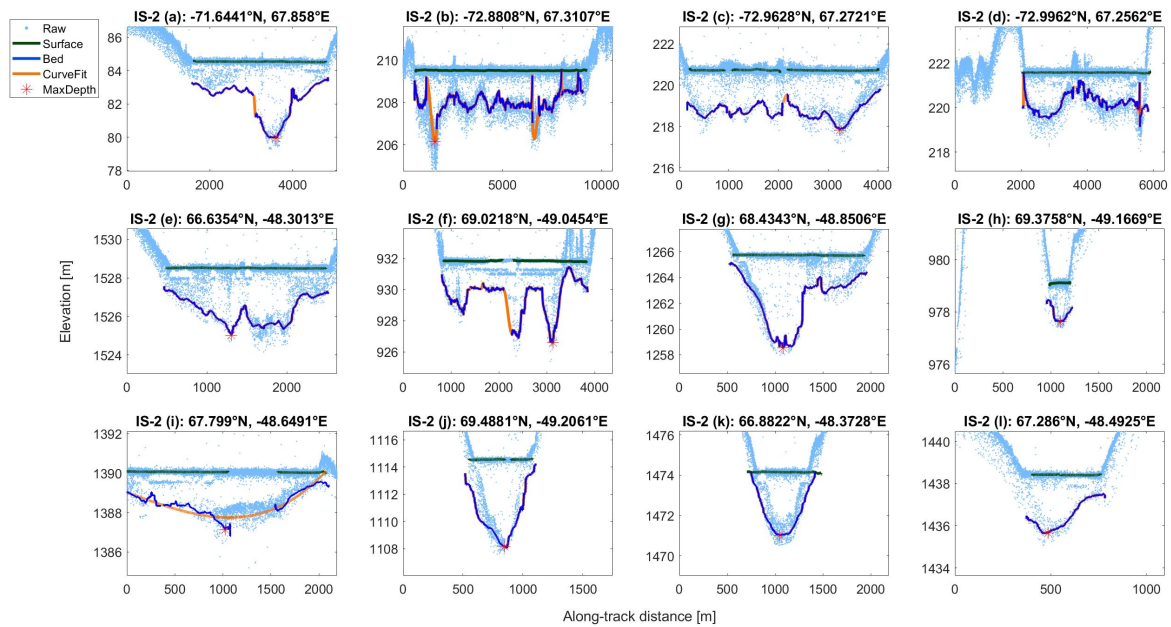


**Figure 4.** Supraglacial lakes and melt ponds detected by ICESat-2 over the Amery Ice Shelf (a-d, first observed by Magruder et al. (2019)) and western Greenland (e-l), using Tracks 0081 and 1222, respectively.

~~Differences in signal confidence between the "land" and "land-ice" surface classifications in the ATL03 algorithm. In both examples, photons received by the lake bottom are labeled as "buffer" photons by the ATL03 algorithm.~~

~~Information on the data used for each altimeter. Altimeter Region Track(s) Date Amery Ice Shelf 0081-2 January, 2019 Jakobshavn Isbræ 1222-17 June, 2019 ATM Hiawatha Glacier 135106-144357-19 July, 2017~~

**Table 1.** Cumulative statistics for ATM supraglacial lakes explored in this study, including mean and maximum signal-based depth ~~for~~ ( $d_s$ ) and polynomial-based depth ( $d_p$ ), along-track extent  $L$ , mean lake depth uncertainty ( $\bar{\sigma}_d$ ), and mean polynomial estimation error ( $\bar{\epsilon}_p$ ). Units are in meters.

Lake	$\bar{d}_s$	$max(d_s)$	$\bar{d}_p$	$max(d_p)$	$L$	$\bar{\sigma}_d$	$\bar{\epsilon}_p$
3a	0.98	1.69	0.91	1.51	270	0.08	0.31
3b	2.25	3.75	2.32	3.49	640	0.15	0.45
3c	1.33	2.39	1.33	2.24	440	0.09	0.25
3d	0.64	0.98	0.71	1.09	180	0.10	0.38
3e	1.81	2.98	2.37	4.11	520	0.05	0.42
3f	1.70	2.70	1.97	3.15	470	0.10	0.49
3g	4.32	7.38	5.50	8.83	630	0.20	1.03
3h	3.64	5.91	3.90	6.37	730	0.15	0.41
3i	1.56	2.38	1.48	2.37	510	0.12	0.15
3j	3.17	5.18	3.39	5.29	650	0.11	0.65
3k	0.60	1.06	0.55	0.97	350	0.09	0.21
3l	1.45	2.32	1.39	2.18	590	0.11	0.15
Mean	1.95	3.23	2.15	3.47	500	0.11	0.41

**Table 2.** As with Table 21, but for ICESat-2 tracks.

Track	Lake	$\bar{d}_s$	$max(d_s)$	$\bar{d}_p$	$max(d_p)$	L	$\bar{\sigma}_d$ <del><math>\bar{\epsilon}_p</math></del>
0081	4a	2.32	4.57	2.62	4.00	3170	0.25 <del>0.60</del>
	4b	1.48	2.67	1.48	1.70	8570	0.80 <del>1.25</del>
	4c	2.02	2.86	2.08	2.41	3790	0.28 <del>0.46</del>
	4d	1.39	2.32	1.46	1.96	3860	0.77 <del>1.21</del>
	<b>Mean</b>	1.80	3.11	1.91	2.52	4850	0.53 <del>0.88</del>
1222	4e	2.24	3.43	2.28	2.98	1990	0.28 <del>0.44</del>
	4f	2.31	5.22	2.66	3.44	2980	0.26 <del>1.07</del>
	4g	3.52	7.15	3.76	5.78	1370	0.49 <del>0.94</del>
	4h	1.22	1.47	1.24	1.50	211	0.12 <del>0.14</del>
	4i	1.52	2.88	1.55	2.37	2070	0.23 <del>0.37</del>
	4j	4.13	6.56	4.13	6.01	530	0.73 <del>0.87</del>
	4k	1.65	3.13	2.04	3.08	780	0.22 <del>0.25</del>
	4l	1.93	2.76	1.93	2.78	360	0.15 <del>0.21</del>
	<b>Mean</b>	2.32	4.08	2.45	3.49	1290	0.31 <del>0.55</del>